

## Advances in NMR Spectroscopy of Weakly Aligned Biomolecular Systems

Sai Chaitanya Chiliveri, Angus J. Robertson, Yang Shen, Dennis A. Torchia, and Ad Bax\*



Cite This: <https://doi.org/10.1021/acs.chemrev.1c00730>



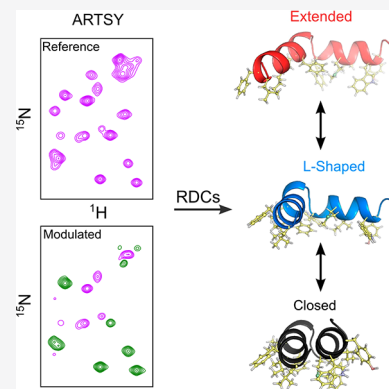
Read Online

ACCESS |

Metrics & More

Article Recommendations

**ABSTRACT:** The measurement and application of residual dipolar couplings (RDCs) in solution NMR studies of biological macromolecules has become well established over the past quarter of a century. Numerous methods for generating the requisite anisotropic orientational molecular distribution have been demonstrated, each with its specific strengths and weaknesses. In parallel, an enormous number of pulse schemes have been introduced to measure the many different types of RDCs, ranging from the most widely measured backbone amide  $^{15}\text{N}$ – $^1\text{H}$  RDCs, to  $^1\text{H}$ – $^1\text{H}$  RDCs and couplings between low- $\gamma$  nuclei. Applications of RDCs range from structure validation and refinement to the determination of relative domain orientations, the measurement of backbone and domain motions, and *de novo* structure determination. Nevertheless, it appears that the power of the RDC methodology remains underutilized. This review aims to highlight the practical aspects of sample preparation and RDC measurement while describing some of the most straightforward applications that take advantage of the exceptionally precise information contained in such data. Some emphasis will be placed on more recent developments that enable the accurate measurement of RDCs in larger systems, which is key to the ongoing shift in focus of biological NMR spectroscopy from structure determination toward gaining improved understanding of how molecular flexibility drives protein function.



### CONTENTS

1. Introduction	A	4.2.2. Impact of Internal Motion	O
2. Alignment Methods	B	4.3. Extracting Dynamics from the RDCs	O
2.1. Liquid Crystals	C	4.3.1. Motions That Do Not Impact Molecular Alignment	O
2.1.1. Phospholipid Bicelles	C	4.3.2. Motions That Impact the Alignment	P
2.1.2. Alkyl-Poly(ethylene glycol)	F	4.3.3. Domain Motions in Paramagnetically Aligned Systems	P
2.1.3. Cetylpyridinium Halide	F	5. Concluding Remarks and Outlook	Q
2.1.4. Filamentous Bacteriophages	F	Author Information	R
2.2. Stretched Acrylamide Gels	F	Corresponding Author	R
2.3. Paramagnetic Alignment	G	Authors	R
2.3.1. Metal-Binding Proteins	G	Notes	R
2.3.2. Alignment by Lanthanide-Binding Tags	G	Biographies	R
2.3.3. Alignment by a Lanthanide-Tagged Fusion Domain	H	Acknowledgments	R
3. Measurement of RDCs	H	References	R
3.1. Backbone Amide $^{15}\text{N}$ – $^1\text{H}$	I		
3.2. $^{15}\text{N}$ – $^{13}\text{C}'$ and $^1\text{H}$ – $^{13}\text{C}'$	J		
3.3. $^{13}\text{C}^\alpha$ – $^{13}\text{C}'$	J		
3.4. $^{13}\text{C}^\alpha$ – $^1\text{H}^\alpha$ and $^{13}\text{C}^\beta$ – $^1\text{H}^\beta$	J		
3.5. $^{13}\text{C}$ – $^1\text{H}$ RDCs in Methyl Groups	L		
3.6. Oligonucleotides	M		
4. Utility of RDCs in Structural Studies	M		
4.1. Structure Calculation	M		
4.2. Structure Validation	N		
4.2.1. Impact of Structural Noise	N		

**Special Issue:** Biomolecular NMR Spectroscopy

**Received:** August 23, 2021

## 1. INTRODUCTION

Solution nuclear magnetic resonance (NMR) spectroscopy is an excellent tool for studying biological macromolecules in both solution and mixed-phase states. This strength derives from the information richness of NMR where each nuclear spin yields its own identifiable signature, either a single resonance or a narrow multiplet, in the NMR spectrum. Crowding and spectral overlap that commonly interfere with spectral analysis can often be resolved by dispersing spectra into two, three, or even four or more orthogonal frequency dimensions.<sup>16–20</sup> The resonance frequencies or chemical shifts report on the immediate chemical environment of the nuclei, and the multiplet structure is largely defined by the local torsion angles.<sup>21–23</sup> Whereas such information often suffices for structural analysis of small organic molecules, the study of protein and nucleic acid structure additionally relies on the ability to map pairwise distances between proximate ( $\lesssim 5$  Å) pairs of hydrogens through the nuclear Overhauser effect (NOE).<sup>24</sup> Nevertheless, because these spectral parameters all report on local structural features, atomic coordinate uncertainty accumulates at greater distances. In contrast, residual dipolar couplings (RDCs) provide information on the orientation of internuclear vectors relative to a global reference frame and are therefore unique complements to the traditional NMR parameters.<sup>6,25–28</sup> Moreover, their exquisite sensitivity to orientation makes them excellent reporters on structural accuracy.

Analogous to dipolar couplings, chemical shift anisotropy (CSA) does not vanish when molecules are weakly aligned.<sup>29</sup> However, since this residual CSA (RCSA) results in a shift of the resonance rather than a change in the multiplet splitting, it requires careful comparison of very small chemical shift differences between aligned and isotropic states. This often poses practical challenges and causes RCSA measurements of proteins to be less common and therefore of less immediate practical interest. Even though RCSAs will not be discussed in this review, they are proving to be powerful parameters for analysis of the stereochemistry in complex organic molecules.<sup>30–32</sup>

The use of dipolar couplings, obtained from strongly oriented samples, as conformational restraints in structure determination has a long history in solid-state NMR.<sup>33–35</sup> Over the past two decades, the analogous but typically much smaller RDCs have been integrated as restraints into conventional protein and nucleic acid structure-determination protocols,<sup>36,37</sup> have been used for the purpose of structure validation,<sup>38,39</sup> and have been exploited to obtain information on intramolecular motions.<sup>4,11,40</sup> The primary hurdle to accessing the richness of structural and dynamics information contained in RDCs is the need to suitably align the molecule of interest. Although a vast array of methods are available to align molecules, each has its own advantages and disadvantages. A second barrier is sometimes posed by the requirement of dedicated software for the analysis of such data, although early useful software is freely available.<sup>41,42</sup> Third, although a large number of pulse sequences have been proposed for the measurement of different types of RDCs, many of these are not included in the standard manufacturer pulse sequence libraries, making the technology less accessible to new users.

Although multiple insightful and in-depth reviews discussing the use of orientational restraints are available,<sup>6,25,26,28,43–45</sup> this review focuses on the practical aspects of RDC acquisition

and computational analysis. Even though the RDCs have become widely used in the study of macromolecular structure, few studies take full advantage of the rich and sensitive structural information they contain. Most investigations limit the measurement of RDCs to a subset of the most easily measured backbone  $^{15}\text{N}$ – $^1\text{H}$  RDCs and use these either for structure refinement, or for structure validation purposes. The latter can be discouraging because RDCs depend strongly on the vector orientation, and even fairly accurate structures can show considerable disagreement with solution RDC data. Frequently, it proves challenging to determine a structural ensemble from traditional NMR restraints that agrees better with the RDCs than an X-ray structure that was determined at a moderate resolution of  $\lesssim 2.5$  Å. However, as highlighted in this review, once alignment suitable for RDC measurement has been achieved, it is straightforward to measure a multitude of different RDC types that all act as independent restraints. Such data then permit determination of a solution structure at considerably improved precision while also allowing for robust validation of the structural accuracy.

Here, we focus only on biomolecular alignment in aqueous systems. However, parallel development of similar technology applicable to organic and bioorganic systems also has undergone tremendous growth in recent years.<sup>46,47</sup> Indeed, development of a wide array of alignment methods compatible with organic solvents,<sup>46,48–56</sup> ingenious new NMR experiments applicable to aligned molecules at natural isotopic abundance,<sup>49,57,58</sup> and novel applications such as determination of stereochemistry have propelled this area of research to new heights.<sup>46,47</sup>

## 2. ALIGNMENT METHODS

Intramolecular nuclear dipole–dipole couplings are proportional to the inverse third power of the internuclear distance. They can be large and are the dominant source of nuclear spin relaxation in biological macromolecules. In a strong external magnetic field, which invariably applies in NMR spectroscopy, only the component of the dipolar field that is parallel to the external magnetic field impacts the resonance frequency of its neighbor. The  $z$  component of the internuclear dipolar field of nucleus  $A$  at the position of a neighbor  $B$  is proportional to the second-order Legendre polynomial  $\{3 \cos^2(\theta_{AB}) - 1\}/2$ , where  $\theta_{AB}$  is the angle between the external magnetic field and the internuclear vector,  $r_{AB}$ . In the absence of an aligning force, all internuclear vectors sample all orientations with equal probability as a consequence of rapid Brownian rotational diffusion. Therefore, the internuclear dipolar coupling averages to zero on a time scale that is faster than the time needed for collecting the free induction decay NMR signal. Consequently, dipolar splittings are absent in NMR spectra of isotropic solutions.

Dipolar couplings have been reintroduced into solution NMR spectra by three commonly used methods: (1) Liquid crystalline solvents<sup>59</sup> or lyotropic phases, i.e., liquid crystalline suspensions of oriented particles; (2) a solvent-rich anisotropic polymer matrix, where the solute interacts only weakly and transiently with the matrix;<sup>60,61</sup> (3) the magnetic susceptibility anisotropy of a molecule,<sup>62–64</sup> which is particularly large for molecules containing a paramagnetic metal ion whose magnetic interaction changes with the orientation of the molecule in the magnetic field. Also worth mentioning is the early work by MacLean and co-workers, who used strong external electric fields to achieve alignment, an approach

usually incompatible with aqueous samples due to their electric conductivity.<sup>65</sup> However, the effect of sample conductivity can be mitigated somewhat by using pulsed, alternating currents to generate the electric fields.<sup>66</sup>

The use of liquid crystalline solvents dates back to the seminal work of Saupe and Englert,<sup>59</sup> who studied solutes in organic liquid crystalline solvents that align cooperatively in an external magnetic field and thereby impose alignment on the solute molecules. Alignment in such solvents typically is very strong, resulting in dipole–dipole couplings that cause splittings of many kHz and often result in extremely complex spectra, even for molecules with less than a dozen nuclear spins.<sup>67</sup> Although elegant multiple quantum NMR experiments can be used to simplify such spectra,<sup>68</sup> in practice it remains very challenging to implement this technology for biomolecules.

In contrast, weakening the degree of solute alignment by several orders of magnitude such that only the largest dipolar couplings remain detectable proved to be a more practical and generally applicable approach. Pioneering work by Bothner-By and co-workers demonstrated that the diamagnetic susceptibility anisotropy of molecules that contain aromatic rings results in a weak degree of alignment that scales with the square of the external magnetic field.<sup>62,69</sup> Incomplete rotational averaging manifested as a change in the corresponding *J* splitting, which represents the sum of the scalar and RDC interactions. Precise measurement of the *J* splitting at different magnetic fields then provides the field-dependent RDC.<sup>69</sup> The magnetic susceptibility anisotropy of molecules that contain a paramagnetic metal can be considerably larger and give rise to RDCs that are easily detectable, as first demonstrated by Prestegard and co-workers for cyanometmyoglobin.<sup>63</sup> However, even for diamagnetic macromolecules, the development of increasingly strong magnets often permits measurement of RDCs without recourse to special alignment agents.<sup>70,71</sup> These RDCs are typically at most a few Hz, and the precision at which they can be confidently measured often becomes a limiting factor. Diamagnetic proteins may be aligned by covalent attachment of a paramagnetic tag, a versatile approach that offers unique opportunities to probe both the structure and the dynamics in multidomain systems (section 2.3.2).<sup>72</sup>

Numerous methods for weakly aligning proteins and nucleic acids have been introduced over the past few decades, with the majority relying on the presence of an anisotropic matrix of inert material that interacts only very weakly with the molecule of interest (Table 1). We refer to this mode of orienting solute molecules as extrinsic alignment. Phospholipid bicelles that can adopt liquid crystalline ordering relative to the magnetic field<sup>107</sup> were the first example of such an alignment medium.<sup>108</sup> Although often depicted as disc shaped, when ordered they have been shown to adopt the morphology of perforated lipid bilayers (Figure 1)<sup>10</sup> that, if neutral, will interact with the solute molecules through a steric occlusion mechanism. In this case, the degree of solute alignment depends on the size and shape of the solute molecule. Predictions made based on the steric alignment model then agree well with observation,<sup>109–112</sup> provided that the solute has no lipophilic character. In addition to the steric mechanism, adding electrostatic charges to the aligning substance introduces an anisotropic electric field in the solvent. Such a field will add an electrostatic energy term that depends on the solute's orientation and therefore will impact the alignment of polar solutes.<sup>110,113,114</sup> A key requirement for all extrinsic alignment

methods is that the solute has no significant affinity for the aligning medium. From an NMR perspective, the latter effectively behaves like a non-tumbling solid and any transient binding to it that lasts for more than a few microseconds will strongly broaden the solute's NMR signals and may also destroy the liquid crystalline order of the aligning matrix. In practice, a primary challenge in carrying out RDC measurements is posed by identifying a medium that yields the desirable degree of solute alignment, optimally yielding <sup>15</sup>N–<sup>1</sup>H couplings in the  $\pm 20$  Hz range for protonated proteins or  $\pm 30$  Hz for perdeuterated proteins. Too weak of an alignment increases the fractional error in the measured RDC; too strong of an alignment detrimentally affects polarization transfer schemes such as INEPT and TROSY, broadens the resonances, and reduces the peak intensity. Of the large array of alignment methods available, below we will focus mostly on methods that have become widely used.

## 2.1. Liquid Crystals

Table 1 presents a compendium of alignment media that confer solute alignment by either steric or electrostatic interaction or both.

**2.1.1. Phospholipid Bicelles.** Magnetic alignment of phospholipid membranes, which relies on the small magnetic susceptibility anisotropy of the individual phospholipids, has a long history.<sup>115–117</sup> In addition to providing information on the dynamics of the lipids, these oriented membranes also proved useful for the study of strongly aligned substances embedded in these membranes, requiring solid-state NMR technology to eliminate the large dipole–dipole interactions.<sup>118</sup> However, such oriented bilayers in an aqueous medium will also confer a very small degree of alignment to both the solvent and any asymmetric solute. Indeed, liquid crystallinity of the aligning medium is commonly judged by monitoring the residual <sup>2</sup>H quadrupolar splitting of the NMR lock solvent. The sharpness of the <sup>2</sup>H doublet components relative to the size of the splitting then reflects the spatial homogeneity of the distribution and alignment of the bilayers across the sample.<sup>75</sup>

Phospholipid bicelles are commonly composed of dimyristoylphosphatidylcholine (DMPC) and the detergent dihexanoylphosphatidylcholine (DHPC), typically at a molar ratio of ca. 3:1.<sup>74,75</sup> However, whereas most detergent is bound to the phospholipid bilayers, where it creates pores analogous to the holes in a slice of Swiss cheese (Figure 1),<sup>10</sup> there remains ca. 5 mM monomeric detergent in solution.<sup>75,119,120</sup> This residual detergent, below its critical micelle concentration of ca. 14 mM, can weakly interact with the solute of interest, as seen for the protein DinI,<sup>121</sup> which can complicate the interpretation of the NMR data.

Either an amphipathic 14-residue peptide<sup>79</sup> or a recently introduced short polymer, styrene maleic acid quaternary ammonium (SMA-QA) polymer,<sup>77</sup> can substitute for DHPC. Furthermore, a novel fructose-based inulin polymer is potentially an even better substitute that, owing to its nonionic amphiphilic character, shows little or no transient binding to many proteins.<sup>78</sup>

DHPC/DMPC bicelles, at the low volume fractions needed to prevent overalignment of proteins, can be difficult to work with because the phase diagram over which the liquid crystalline ordering occurs is very sensitive to the relative concentration of DHPC:DMPC.<sup>75,119</sup> The required molar ratio changes from ca. 1:3.5 for concentrated samples (>10%

Table 1. Methods for Weakly Aligning Proteins and Nucleic Acids Relative to the Magnetic Field

method	common name	components	charge	detergent compatible	temperature range (°C)	pH range	widely used	remarks	ref
liquid crystal	bicelles	DMPC/DHPC	neutral	no	27–45	6–7	+	prone to hydrolysis at low and high pH; CTAB/SDS stabilize alignment	39,73,74
		DMPC/DHPC/CTAB	positive						
		DMPC/DHPC/SDS	negative						
		DTPC/DHPC	neutral	no	20–50	6–7	–	extends temperature range to lower values	39,75
		DTPC/DHPC/CTAB	positive						
		DLPC/CHAPSO	neutral	no	7–50	NR <sup>a</sup>	–	extended temperature range	76
	polymer bicelles	DMPC/SMA-QA	positive	no	30–45	2.5–10	–	requires chemical synthesis	77,78
	polypeptide bicelles	DMPC/polypeptide	neutral	no	30–45	NR <sup>a</sup>	–	requires synthetic peptide	79
	ether bicelles	DTPC/DIOHPC	neutral	no	32–46	1–12	–	chemically stable but expensive	39
		DIODPC/CHAPSO	neutral	no	10–60	1–6.5	–	chemically stable but expensive	80
	PEG	<i>CmEnI/n</i> -hexanol	neutral	no	0–40	insensitive to pH	++	inexpensive; low binding affinity for biomolecules	81,82
		<i>CmEnI/n</i> -hexanol/CTAB	positive						
	cetylpyridinium halide	cetylPrBr/ <i>n</i> -hexanol/NaBr	positive	no	15–60	2.2–8	–	inexpensive; slow to align	83
		cetylPrCl/ <i>n</i> -hexanol/NaCl	positive	no	0–70	2.2–8	–	best at high ionic strength (200 mM NaCl)	84
	pinacyanol	pinacyanol acetate	positive	yes	15–60	3–11	–	incompatible with NaCl > 50 mM	85
	squalamine	squalamine	positive	no	1–40	4–8	–	best at ionic strength < 50 mM	86
	viral suspension	Pf1	negative	no	10–45	5 and above	+++	commercially available; easy to use	87,88
		fd	negative	yes	5–60	3 and above	–	easy to use	89,90
		TMV	negative	no	5–60	5 and above	–	easy to use	89
	rat tail tendon type I collagen	collagen	neutral	yes	25–42	6–8	–	slow to align in the magnetic field	91
	cellulose nanocrystals	cellulose	negative	yes	10–70	2.5–8	–	compatible with nonionic detergents	92,93
	DNA nanotubes	mixture of M13 bacteriophage ssDNA and synthetic ssDNA	negative	yes	30 (range NR <sup>a</sup> )	NR <sup>a</sup>	–	expensive; suitable for negatively charged biomolecules	94
	K <sup>+</sup> -d(GpG)	G-tetrad DNA	negative	yes	10–37	5.8–8	–	commercially available only as sodium salt of d(GpG)	95
	flagella	<i>Chlamydomonas reinhardtii</i> flagella	negative	yes	4–40	4–8	–	obtained from deflagellation of <i>C. reinhardtii</i>	96
	purple membrane	purple membrane	negative	no	0–70	2.5–10	–	solute alignment is dominated by electrostatics; very dilute PM concentrations can suffice	97–99
	2D crystalline fragments of lipids and bacteriorhodopsin								
	paramagnetic alignment	purple membrane with Tb <sup>3+</sup> paramagnetic lanthanide ion					–	line broadening in proximity to lanthanide ion; alignment increases with square of B <sub>0</sub> .	11,100
	lanthanide ion replacement	paramagnetic lanthanide ion					–	same as above	101,102
	extension by lanthanide-binding EF-hand	paramagnetic lanthanide ion					–	alignment increases with square of B <sub>0</sub> ; additional GB3 resonances; generation of near-orthogonal alignment	103
	extension by lanthanide-bound GB3	paramagnetic lanthanide ion					–	alignment increases with square of B <sub>0</sub> ; best tags require custom synthesis	72,104,105
	engineered Cys lanthanide-binding tag	paramagnetic lanthanide ion					++		

Table 1. continued

method	common name	components	charge	detergent compatible	temperature range (°C)	pH range	widely used	remarks	ref
stretched/compressed hydrogels	polyacrylamide	acrylamide	neutral	yes	5–45	pH insensitive	+	high compatibility with biomolecules; careful handling required due to strong osmotic swelling forces	60,61,106
		acrylamide/acrylate	negative	yes	5–45	NR <sup>a</sup>	+		
		acrylamide/AMPS	negative	yes	5–45	NR <sup>a</sup>	+		
		acrylamide/DADMAC	positive	yes	5–45	NR <sup>a</sup>	+		

<sup>a</sup>Not reported.

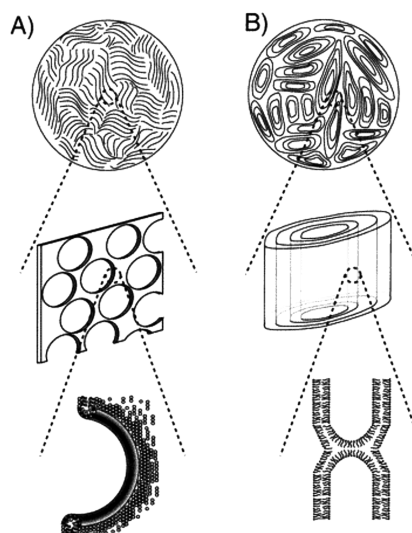


**Figure 1.** Morphology of three different types of lyotropic liquid crystalline media: (A) Ordered bicelles; (B) PEG/*n*-hexanol. Top views depict slices orthogonal to the NMR sample tube, which has its axis parallel to the magnetic field. Lower panels illustrate (A) the pores in the DMPC bilayer with the rims covered by detergent and (B) a bridge-type structure between bilayers in the PEG/*n*-hexanol medium. (Reprinted with permission from ref 10. Copyright 2001 American Chemical Society).

w/v) to less than 1:3 for more dilute samples (<5% w/v) because for dilute bicelle samples a larger fraction (ca. 5 mM) exists in the monomeric state in fast equilibrium with the DMPC-bound state. Considerable stabilization of the liquid crystalline phase can be obtained by doping the bilayers with positively or negatively charged amphiphiles, causing electrostatic repulsion between the bilayers. Both cetyltrimethylammonium bromide (CTAB; positive) and sodium dodecyl sulfate (SDS; negative) are commonly used for this purpose<sup>74</sup> at mole fractions ranging from ca. 1% to as high as 30% relative to DMPC. The temperature range over which the sample remains stable can be adjusted by changing the length of the alkyl chain: substituting DMPC by ditridecanoyl-phosphatidylcholine, which has a lower melting temperature, decreases the low-temperature limit over which the samples remain liquid crystalline from ca. 30 to 22 °C.<sup>75</sup> Shortening the alkyl chain length of the lipid to 12 carbons and changing the detergent to CHAPSO extends the temperature range even further (Table 1).<sup>76</sup> Hydrolysis of the phospholipid diester bond is both acid and base catalyzed and may be accelerated by multivalent metal ions.<sup>122</sup> A metal chelator, such as ethylenediaminetetraacetic acid (EDTA), may mitigate this effect while simultaneously suppressing bacterial growth.<sup>123</sup> Bicelle samples are chemically most stable at pH 6.5 unless DHPC is substituted by dihexylphosphatidyl choline (DI-OHPC), which allows prolonged measurements over a wide pH range.<sup>39</sup>

Although bicelles, either DMPC/DHPC or the polymer-stabilized DMPC/SMA-QA,<sup>77</sup> are often depicted as nanodiscs, it is important to realize that the nanodisc model only applies in the more dilute region of the phase diagram where they do not result in liquid crystalline alignment. Above the threshold concentration where they switch to liquid crystalline ordering they have a morphology of perforated bilayers with the detergent (or the SMA-QA or inulin polymers) lining the rims of the pores.<sup>10</sup>

**2.1.2. Alkyl-Poly(ethylene glycol).** A less expensive and sometimes more robust medium for aligning proteins or other biomolecules is based on the use of *n*-alkyl-poly(ethylene glycol)/*n*-alkyl alcohol mixtures.<sup>81,124</sup> These short alkyl-poly(ethylene glycol) polymers are commonly denoted as *CmEn*, where *m* is the number of carbons in the *n*-alkyl group and *n* is the number of glycol units in the poly(ethylene glycol) moiety.<sup>124</sup> C12E5 and C8E5 are the most widely used and cover the above and below room-temperature regions, respectively. Usually *n*-hexanol is used for the alcohol with C12E5 and *n*-octanol with C8E5 in fairly tightly defined molar ratios of polymer to *n*-hexanol or *n*-octanol (ca. 0.85–1.0).<sup>81</sup> These amphiphiles are reported to adopt a dilute lamellar  $L_{\alpha}$  liquid crystalline phase that aligns with the bilayer normal orthogonal to the magnetic field. Tracer diffusion measurements indicate the presence of considerable imperfections in this model under the conditions where NMR measurements are carried out (Figure 1B),<sup>10</sup> but the liquid crystalline ordering is not as prone to perturbation by proteins immersed in such suspensions than the less robust DHPC/DMPC bicelles. Small molar fractions of charged amphiphiles such as SDS are very useful to further increase the stability of the  $L_{\alpha}$  phase.<sup>125</sup>

**2.1.3. Cetylpyridinium Halide.** Cetylpyridinium halide solutions in water in the presence of a 1:1.33 (w/w) fraction of hexanol will adopt a lamellar Helfrich phase suitable for the alignment of proteins.<sup>83,84</sup> Reportedly, the use of bromide over chloride is advantageous in yielding homogeneously stable liquid crystalline aligned bilayers over a wide range of temperatures, ionic strengths, and pHs.<sup>83</sup> Due to the high net surface charge of the bilayer, electrostatic interaction with the solute often dominates the alignment, and the medium appears to be most suitable for proteins that are nearly neutral or carry a net positive charge. The liquid crystalline alignment can take many hours to become fully established when placed in the magnetic field.

**2.1.4. Filamentous Bacteriophages.** The most widely used alignment medium is a dilute suspension of the filamentous bacteriophage Pf1.<sup>87</sup> Three strong advantages of Pf1 are that (1) it is commercially available (Asla Biotech, Latvia), (2) it is compatible with the majority of water-soluble biomolecules, (3) and a small amount from a concentrated stock solution can simply be pipetted and mixed into the sample of interest. Other phages, including *fd* and tobacco mosaic virus, have also been used for alignment but much less frequently.<sup>89</sup> Pf1 is worm shaped with a contour length of ca. 2  $\mu\text{m}$  and a diameter of 67 Å.<sup>126</sup> It carries a rather strong negative surface charge of ca. 0.46 e/nm<sup>2</sup>.<sup>127</sup> This net negative charge enhances its effective diameter and causes a suspension of such phages to adopt liquid crystalline order at concentrations as low as a few mg/mL.<sup>87,128</sup> The negative surface typically results in a degree of solute alignment that is much larger than would be predicted based on just the shape of the solute, and indeed, solute alignment is often dominated by the solute's electric dipole and quadrupole moments interacting with the electric field surrounding the magnetically oriented phage particles.<sup>114</sup> For proteins that align too strongly, even at dilute Pf1 concentrations, addition of salt can be used to weaken the electrostatic component of the alignment.<sup>128</sup> At high salt and low Pf1 concentration, the ordering of Pf1 becomes paranematic and increases with magnetic field strength.<sup>128</sup> Below a critical threshold concentration, which increases with ionic strength, samples

can also phase separate, resulting in a lower sample fraction that is nematic and an upper fraction that is isotropic. Such phase separation is usually seen by visual inspection of the sample and leads to superimposed singlet and quadrupolar split <sup>2</sup>H lock signals. Such phase separation is more common for phages such as *fd* that have a contour length much shorter than Pf1.

## 2.2. Stretched Acrylamide Gels

For some proteins, it can be difficult or even impossible to find a liquid crystalline medium that offers adequate conditions for measurement of RDCs. This may apply to proteins that require detergents for solubility because surfactants often destructively interfere with the liquid crystals (Table 1). For such systems, the use of "strain-induced alignment in a gel" (SAG) is a robust and inexpensive alternative to obtain the required degree of solute alignment.<sup>60,61</sup> Polyacrylamide is a rather inert material with low or no detectable affinity for most proteins or nucleic acids, and importantly, it is also compatible with detergents. By casting gels that are sufficiently dilute in polymer concentration (typically <10% w/v; preferably  $\leq 5\%$  w/v), the solute will diffuse in the aqueous solution while experiencing transient steric interactions with the polymers. By stretching the gels inside the NMR sample tube, the orientation of the polymers has a small preference to be parallel to the magnetic field. The transient steric interactions then impose a preferential degree of order on the solute such that its long axis has a slight preference to be parallel to the magnetic field, conceptually analogous to the steric alignment model originally developed for bicelles.<sup>109</sup>

There are many advantages to this method of aligning proteins and nucleic acids. First, the strength of the alignment can be tuned by the degree of stretching applied to the gel. In practice, this is achieved by casting the gel in a cylinder that is larger than the inner diameter of the NMR tube followed by the use of a funnel to push the gel into an open-ended NMR tube that is then sealed at the bottom with no air gap between the gel and the closing plug.<sup>129</sup> Typically, the maximum achievable radial compression results in a diameter reduction from a casting diameter of ca. 5.6 mm to the 4.2 mm inner diameter of a standard NMR tube, which corresponds to stretching of the gel by a factor of ca. 1.78. At higher compression factors, the gel is prone to crack when inserted into the NMR tube. If alignment is too strong, either the gel can be cast inside a smaller diameter cylinder or the percentage of acrylamide can be lowered, in practice to as low as ca. 4% w/v for neutral polyacrylamide.

A very useful addition to the use of acrylamide gels is the incorporation of negative or positive charges. Most commonly used are acrylic acid or 2-acrylamido-2-methyl-1-propane-sulfonic acid (AMPS) for charging the gels negatively or either 3-acrylamidopropyl-trimethylammonium chloride (APT-MAC)<sup>130</sup> or diallyldimethylammonium chloride (DAD-MAC)<sup>131</sup> for adding positive charge. After casting such gels at a relatively high ionic strength, they are soaked in distilled water for several days prior to dehydrating in the same manner as that used for the neutral gels,<sup>60,61</sup> followed by soaking the dehydrated, shrunken gel into the protein or nucleic acid solution of interest. An important advantage of using charged or partially charged gels is that osmotic pressure causes swelling of the gel during this final soaking to a diameter that will be larger than the casting diameter, offering the possibility to decrease the final gel fraction of the NMR sample to well

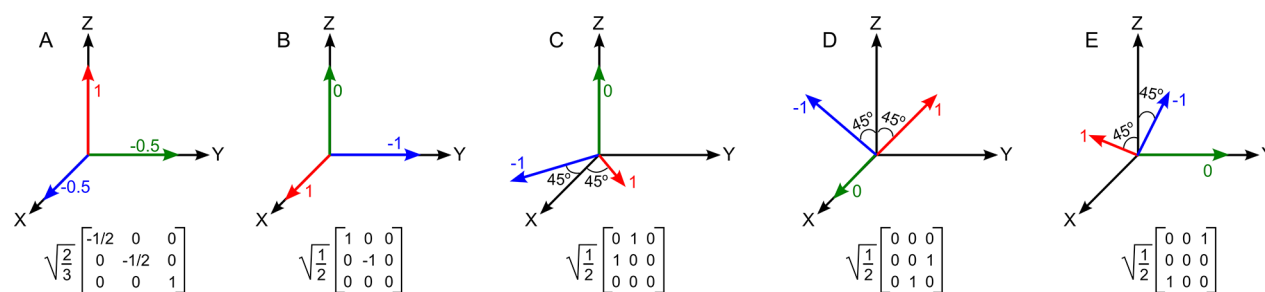


**Figure 2.** Schematic depiction of five orthonormal alignment tensors and their corresponding Saupe matrices. Alignment tensor orientation and its principal component relative sizes are indicated in color, and the molecular coordinate frame is in black, chosen to coincide with that of the axially symmetric alignment tensor in A. All other tensors are fully rhombic.

below 4%. This osmotic swelling therefore enables the use of lower fractions of polymer, thereby mitigating one of its main disadvantages that the presence of polymers in the sample will reduce the rate of Brownian rotational diffusion, as manifested in faster transverse relaxation.<sup>61</sup> The charged gels also tend to accelerate the soaking process and are less prone to slow shrinkage along the long axis after insertion into the NMR sample tube.

The polymer can yield strong NMR signals in the downfield region of the NMR spectrum that result in excessive  $t_1$  noise ridges.<sup>124,132</sup> This  $t_1$  noise can be effectively suppressed by gradient-encoded, sensitivity-enhanced detection techniques,<sup>133</sup> which are compatible with most of the common pulse schemes used for measurement of RDCs.

### 2.3. Paramagnetic Alignment

As first demonstrated by Prestegard and co-workers for cyanometmyoglobin,<sup>63</sup> the magnetic susceptibility anisotropy of paramagnetic metals tightly chelated to a protein or nucleic acid generally will result in weak alignment that suffices for accurate RDC measurement. The degree of alignment, and thereby the RDC, increases with the square of the magnetic field strength but typically falls in a range for convenient use at common field strengths in the 500–900 MHz range. A disadvantage of paramagnetism-induced alignment is that  $^1\text{H}$  signals within a radius of ca. 10–20 Å, depending on the metal, are severely broadened by paramagnetic relaxation, which limits the number of internuclear RDC measurements. However, as discussed below, there are multiple ways to mitigate this problem. Importantly, paramagnetic alignment offers unique opportunities to quantitatively evaluate the amplitude and direction of domain motions in multidomain proteins (see section 4.3.3).

**2.3.1. Metal-Binding Proteins.** Metalloproteins, where either the natural paramagnetic metal has an anisotropic electron distribution or a lanthanide can be substituted for the natural metal, can be aligned in a magnetic field without recourse to gels or liquid crystals. Examples are cyanometmyoglobin<sup>63</sup> and calmodulin, where one or more of the  $\text{Ca}^{2+}$ -binding sites can be mutated to selectively bind a lanthanide ion such as  $\text{Tb}^{3+}$  or  $\text{Tm}^{3+}$ .<sup>11</sup> Because the paramagnetic metal is typically held captive in the protein's interior, the number of sites obscured by paramagnetic relaxation can be substantial. However, many of the modern applications and further developments of weakly aligned proteins were based on the pioneering work that involved natural metal-binding proteins.<sup>11,63</sup> Notably, there is a large variation in the magnetic susceptibility anisotropy among the lanthanides, and the use of different lanthanides for the same protein can substantially

alter the orientation and magnitude of the protein's alignment.<sup>134,135</sup>

**2.3.2. Alignment by Lanthanide-Binding Tags.** The earliest and often easiest way to obtain paramagnetic alignment of proteins that normally do not bind metals tightly is to extend them at either the N- or the C-terminus by a short metal-binding peptide, commonly of the EF-hand type found in  $\text{Ca}^{2+}$ -binding proteins.<sup>101</sup> The affinity of such tags for lanthanides is typically in the low nanomolar range, which enables the investigation of exchange between metal-free and metal-bound species so that the paramagnetic and diamagnetic resonances can be linked by  $zz$  spectroscopy.<sup>136</sup> Covalent attachment of a very tightly metal-chelating prosthetic group to a protein or nucleic acid provides an attractive alternative.<sup>72,135,137</sup> A range of tags, all with very high affinity for lanthanides, has been introduced for this purpose and are commercially available.<sup>104,135</sup> However, they frequently are present as different stereochemical isomers that are in slow chemical equilibrium with one another, giving rise to different alignment orientations that can complicate spectral analysis. Moreover, the use of relatively long and flexible linkers between such commercial tags and the protein can reduce the alignment. A custom-synthesized tag, often referred to as M8Spy, can greatly alleviate both of these problems<sup>105</sup> provided  $\text{Tm}^{3+}$  or  $\text{Yb}^{3+}$  is used as the paramagnetic lanthanide.<sup>138</sup> A more recently introduced M7PyThiazole-DOTA tag also appears to be very useful.<sup>139</sup> Such lanthanide-binding tags are covalently attached to the sulfur atom of a surface-accessible Cys residue. Generation of Cys substitutions at different sites also yields different alignment orientations, in principle making it possible to generate up to five linearly independent alignment tensors (Figure 2).<sup>103</sup> Although highly desirable for probing the amplitude and direction of internal motion from the RDCs, available through such "orthogonal" alignments,<sup>5</sup> in practice it can be very challenging to design the mutants that optimize orthogonality. Moreover, resonances from protons that are proximate ( $\lesssim 15$  Å) to the lanthanide will be paramagnetically broadened and therefore attenuated, often below the detection limit. Pseudocontact shifts (PCS) induced by the paramagnetic ion can present an additional challenge because assigning the tagged protein may require additional experiments and/or advanced software.<sup>140–142</sup> On the other hand, PCS have long been recognized as an important source of structural information, and the restraints obtained from such work can be highly beneficial.<sup>143–145</sup>

For nucleic acids, the commercial availability of the phosphoramidite derivative, dT-EDTA, makes it straightforward to incorporate a lanthanide-binding tag into synthetic DNA,<sup>146</sup> offering the opportunity to align protein–nucleic

complexes and extract unique information on both structure and dynamics.<sup>146</sup>

**2.3.3. Alignment by a Lanthanide-Tagged Fusion Domain.** An elegant solution for obtaining multiple “orthogonal” alignments of a protein can be achieved by expressing it as a fusion construct with a small GB3 domain (56 residues) that is sometimes used to promote protein expression prior to cleavage of the linker and purification<sup>147</sup> or that can be left attached to promote protein solubility.<sup>148</sup> Yao and co-workers designed a set of five GB3 Cys mutants that, following attachment of a lanthanide tag such as M8Spy, yield a set of remarkably independent alignment tensors for GB3 and thereby for the fused protein of interest.<sup>103</sup> An advantage of this approach over directly tagging the protein is that the lanthanide is further away, thereby strongly reducing the effects of both paramagnetic line broadening and pseudocontact shifts, in particular for the K19C and V21C GB3 mutants where the lanthanide is quite distant from the target protein. A disadvantage is that the total size of the protein and thereby the spectral complexity as well as the rotational correlation time ( $\tau_c$ ) are increased. Because of flexibility in the linker between GB3 and the protein of interest, the alignment of the latter will be weaker than the alignment of GB3, but at 900 MHz it was sufficiently strong to allow for facile and precise measurement of RDCs.<sup>103</sup> GB3, expressed as a fusion construct, is isotopically enriched, and its resonances result in additional crowding. Although this approach has not yet been widely explored, the availability of high-quality amide RDCs under multiple, very different alignments holds unique potential for detailed characterization of domain motions as well as *de novo* structure determination.

### 3. MEASUREMENT OF RDCS

An important question is how many RDCs are required to determine the structure of a protein? In part, this question can be answered by the number of parameters needed to define a protein backbone: Assuming an idealized covalent geometry and planarity of the peptide bonds, just two parameters per residue,  $\varphi$  and  $\psi$ , are needed to define the structure of a polypeptide chain. This argument suggests that two independent backbone RDCs per residue could suffice. Such RDCs could be measured either for a single type of interaction, e.g.,  $^1D_{\text{NH}}$ , under conditions of very different alignment, or for vectors that have very different orientations, such as  $^1D_{\text{NH}}$  and  $^1D_{\text{NC}}$  or  $^1D_{\text{CaC}}$ . Here, different alignment is defined by a scalar product that is much smaller than 1 for the five-dimensional vectors of unique Saupe matrix elements, applicable to the two alignment conditions.<sup>97</sup> Therefore, in principle, one might expect that the accurate measurement of two very different types of RDC per peptide unit or a single type of RDC under very different alignment conditions should suffice to define a protein backbone structure.

In practice, however, the answer is more complex. First, there is a 2-fold degeneracy in linking an RDC to the corresponding vector orientation as a given RDC cannot distinguish a vector from its inverse direction (Figure 3). Second, small deviations from the idealized geometry can have large effects on the value of the RDCs.<sup>131</sup> Third, measurement errors and incompleteness complicate the analysis. Fourth, both the amplitudes and directions of internal motions relative to the alignment tensor impact the RDCs. Another very challenging problem is posed by the multipitted energy surface when searching for a structure that is simultaneously

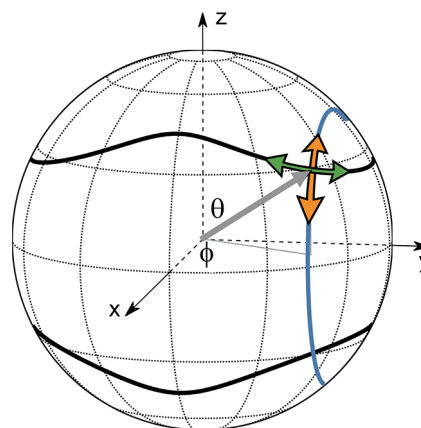


**Figure 3.** Orientations of an internuclear vector (gray) compatible with an experimental RDC measured under two different alignment orientations, depicted by the black and blue cones. A single RDC value cannot uniquely define both polar coordinates,  $\theta$  and  $\varphi$ , but a second RDC measurement reduces the degeneracy to a discrete number (8 for this example) of orientations. Oscillations of vector orientations on the black cone surface (green) will not change the RDC, but oscillations depicted by the orange arrows will impact the value. The inverse applies for the alignment depicted by the blue cone. Measurements under five linearly independent alignment conditions can map the direction and amplitudes of such excursions.<sup>4–6</sup>

compatible with all of the RDCs. Hence, it is easier to refine a structure<sup>36,149,150</sup> that is already fairly close to its true, time-averaged state than to determine it *de novo*, and the use of such refinement protocols is far more common than applications that build a structure from the RDCs alone.<sup>151,152</sup> Recent developments in molecular modeling may generate *de novo* structural models whose accuracy is on par with that of good-quality X-ray structures and therefore may provide starting models suitable for refinement with experimental RDC data.<sup>153–155</sup> To improve the structural quality, it is highly desirable to measure more than just two high-quality backbone RDCs per residue, which requires either generation of multiple independent alignment conditions or measurement of multiple types of RDCs in a single alignment medium. Considering that the generation of multiple independent alignment conditions that a given biochemical system will tolerate is often a challenging endeavor, measurement of the different types of RDCs in a single alignment medium is generally more straightforward and less demanding in terms of sample preparation. This section reviews the measurement of such RDCs on  $^{15}\text{N}$ -,  $^{13}\text{C}^{15}\text{N}$ -, and  $^2\text{H}^{13}\text{C}^{15}\text{N}$ -labeled biomolecules.

The RDCs can be measured between any pair of spatially proximate spin-1/2 nuclei, including  $^1\text{H}$ – $^1\text{H}$ ,  $^1\text{H}$ – $^{15}\text{N}$ ,  $^1\text{H}$ – $^{13}\text{C}$ ,  $^{13}\text{C}$ – $^{13}\text{C}$ , and  $^{15}\text{N}$ – $^{13}\text{C}$ . Although many types of  $^1\text{H}$ – $^1\text{H}$  RDCs can readily be measured,<sup>108,156,157</sup> those that involve fixed  $^1\text{H}$ – $^1\text{H}$  distances (e.g., interproton couplings in methylene and methyl groups or  $^1\text{H}^\delta$ – $^1\text{H}^\epsilon$  couplings in Tyr) are more straightforward to interpret because they only depend on the orientation. However, these fixed distance  $^1\text{H}$ – $^1\text{H}$  RDCs have not been used widely and therefore will not be discussed here. Instead, we focus on heteronuclear couplings (Figure 4) that are easily measured at high precision and that are applicable to intermediate sized protein ( $\lesssim 50$  kDa), typically studied by NMR.

Generally, there are two strategies to measure RDCs: (1) direct measurement from an observed splitting, usually

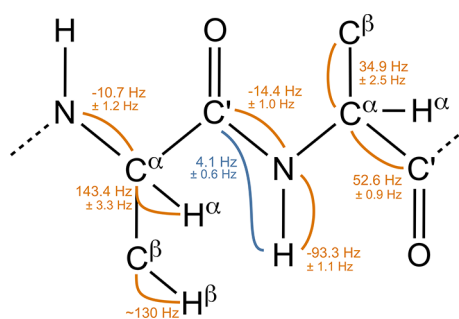


**Figure 4.** Schematic depiction of RDCs that are readily measured at good precision in isotopically enriched proteins. RDCs manifest as changes in the corresponding one-bond  $J$  couplings, whose average value and standard deviation are marked in orange.<sup>1–3</sup> Blue marks the two-bond  $^{13}\text{C}'\text{--}^1\text{H}^n$  interaction, which also can be very useful and is best measured in perdeuterated proteins.

representing the sum of the  $J$  coupling and the RDC; (2) measurement of the relative signal amplitude in spectra recorded with different dephasing delays preceding the acquisition. Method 1 is perhaps the simplest because it essentially relies on conventional spectral analysis to measure splittings, but it suffers from a doubling of the number of resonances relative to a decoupled spectrum, thereby halving the sensitivity. Method 2, sometimes referred to as quantitative  $J$  correlation,<sup>158</sup> encodes the coupling into the intensity of the decoupled resonance. The advantage of this approach is spectral simplicity, but it requires a minimum of two spectra: a reference spectrum and a spectrum where resonances are attenuated due to dephasing. This latter method is typically less demanding in terms of the sample concentration needed to achieve a given accuracy of the measured coupling. However, small systematic errors can result when isotopic enrichment is incomplete or when timing delays or pulse widths have not been properly optimized. Such systematic errors are strongly reduced when both the isotropic  $J$  values and the  $J + D$  splittings of the aligned sample are measured back-to-back with identical settings, because systematic errors affect both measurements comparably and are therefore greatly diminished when the RDC is derived from their difference.

### 3.1. Backbone Amide $^{15}\text{N}\text{--}^1\text{H}$

One-bond  $^{15}\text{N}\text{--}^1\text{H}$  RDCs were the first to be measured experimentally in a protein<sup>63</sup> and remain the most widely used type of coupling.  $^{15}\text{N}$  transverse relaxation is relatively slow, resulting in narrow  $^{15}\text{N}$  line widths and permitting  $^1J_{\text{NH}}$  or  $^1J_{\text{NH}} + ^1D_{\text{NH}}$  splittings to be measured at good precision in the  $^{15}\text{N}$  dimension when  $^1\text{H}\text{--}^{15}\text{N}$  HSQC spectra are recorded without  $^1\text{H}$  decoupling during  $^{15}\text{N}$  evolution. The increase in resonance overlap that can result from the doubling of the number of resonances can be reversed by recording two spectra in an interleaved mode, where one yields in-phase (IP) and the other antiphase (AP)  $^{15}\text{N}\text{--}\{^1\text{H}\}$  doublets. The sum and difference of the IP and AP spectra will yield only the downfield or upfield doublet component, resolving the spectral crowding.<sup>159</sup> However, the simplicity of this IPAP-type measurement is somewhat deceptive because unresolved multibond couplings together with cross-correlated relaxation can adversely impact the accuracy of such measurements unless a more advanced pulse scheme is used.<sup>160</sup> Also, because relaxation interference between the  $^{15}\text{N}\text{--}^1\text{H}$  dipolar interaction and the  $^{15}\text{N}$  chemical shift anisotropy (CSA) causes the upfield

$^{15}\text{N}\text{--}^1\text{H}$  doublet component to be much broader and weaker than the downfield one, measurement of the peak position of this “anti-TROSY” component becomes less precise (see below). Therefore, in practice, this IPAP-HSQC experiment is not suitable for proteins with  $\tau_c \gtrsim 10$  ns.

The accuracy at which a splitting can be measured is limited by the uncertainty ( $\epsilon_p$ ) in the peak position. An empirical lower limit for this uncertainty is obtained by peak picking synthetic spectra with Lorentzian line shapes in the presence of Gaussian noise when using a robust algorithm that fits the discrete points of a resonance above its half height to a Lorentzian<sup>161</sup>

$$\epsilon_p \approx 0.5 \times \text{LW}/(\text{S/N}) \quad (1a)$$

where LW is the line width at half height and S/N is the signal-to-noise ratio of that resonance. If both doublet components have comparable intensities, the uncertainty in the splitting will be  $\sqrt{2}$  larger. Assuming the S/N of the isotropic spectrum is comparable to that of the aligned spectrum, the uncertainty in the isotropic  $J$  splitting will be of similar magnitude. Therefore, a reasonable estimate for the uncertainty in the RDC,  $\epsilon_{\text{RDC}}$ , derived from the difference in the doublet splittings, is given by

$$\epsilon_{\text{RDC}} \approx \text{LW}/(\text{S/N}) \quad (1b)$$

An elegant alternative to deriving couplings from the measurement of peak positions relies on measuring the  $^1J_{\text{NH}} + ^1D_{\text{NH}}$  dephasing that occurs during a  $^{15}\text{N}$  constant-time evolution period<sup>162</sup> or, more generally, fitting the amplitude of resonances that have been subjected to variable durations of  $J$ -dephasing. This type of measurement can yield very precise values and was used to measure the minute RDCs in ubiquitin (in the range from  $-0.1$  to  $+0.2$  Hz at 600 MHz) resulting from the protein’s magnetic susceptibility anisotropy<sup>64</sup> and also for its approximately 3-fold larger  $^{13}\text{C}\alpha\text{--}^1\text{H}\alpha$  RDCs at 750 MHz.<sup>163</sup> However, in practice, such extreme precision is rarely required and much simpler alternatives that rely on the same principle can be used.

The so-called ARTSY (Amide RDCs by TROSY) pulse sequence represents perhaps the most convenient method for measuring the amide RDCs by quantitative  $J$  correlation.<sup>9</sup> This experiment records two interleaved  $^1\text{H}\text{--}^{15}\text{N}$  TROSY-HSQC spectra, where the first INEPT transfer duration,  $\tau$ , either is the standard value ( $\tau_{\text{ref}} = 5.435$  ms) or is lengthened to a value that would be expected to yield a null if  $^1J_{\text{NH}} + ^1D_{\text{NH}} = 92$  Hz ( $\tau_{\text{att}} = 10.87$  ms). This method relies on incomplete rephasing of the  $^1\text{H}^n\text{--}\{^{15}\text{N}\}$  doublet components when the INEPT duration,  $\tau$ , is set to  $1/J_{\text{NH}}$  due to the additional effect of  $^1D_{\text{NH}}$ . The experiment is best suited for perdeuterated proteins that are less impacted by dephasing from  $^1\text{H}\text{--}^1\text{H}$  couplings during the  $\tau$  interval but can be adapted to fully protonated proteins by using an amide-selective  $180^\circ$  pulse.<sup>9</sup> Due to the line narrowing afforded by the TROSY detection scheme,<sup>164</sup> the ARTSY spectra offer excellent resolution and sensitivity, in particular, when recorded at high magnetic field strengths. Resolution can be further enhanced by applying the same encoding scheme to the sensitive TROSY-HNCO experiment.<sup>165</sup> Spectra are then well resolved and applicable to proteins as large as the SARS-CoV-2 main protease, a 68 kDa homodimeric enzyme (Figure 5).

The uncertainty in the ARTSY-derived  $^1J_{\text{NH}} + ^1D_{\text{NH}}$  splitting is inversely proportional to the S/N of the resonance

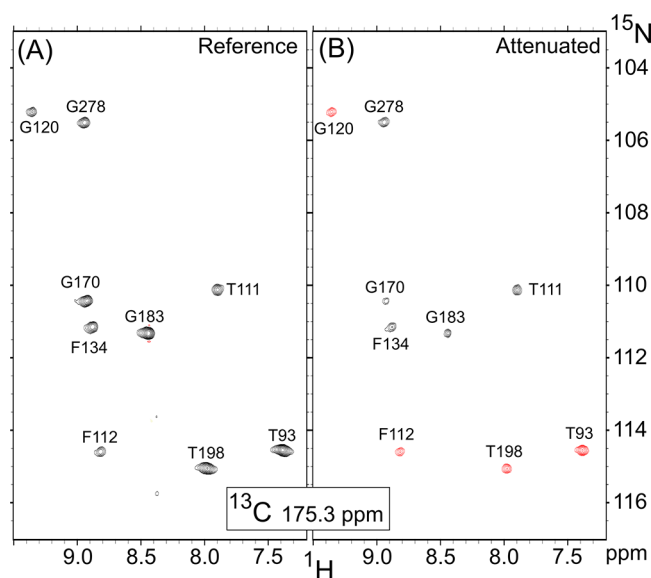


**Figure 5.**  $^1\text{H}$ – $^{15}\text{N}$  cross sections through the 900 MHz 3D ARTSY-HNCO spectrum of the perdeuterated homodimeric main protease of SARS-CoV-2 (68 kDa), aligned in 11 mg/mL Pfl. Magnitude of  $^1J_{\text{NH}} + ^1D_{\text{NH}}$  is derived from the intensity ratio of peaks in the attenuated ( $I_{\text{att}}$ ;  $2T$  dephasing) and reference ( $I_{\text{ref}}$ ;  $T$  dephasing;  $T \approx 5.4$  ms) spectra according to  $^1J_{\text{NH}} + ^1D_{\text{NH}} = (2/\pi T)\cos^{-1}(I_{\text{att}}/2I_{\text{ref}})$ .

in the reference spectrum and is approximately given by  $30/(S/N)$ .<sup>9</sup>

The ARTSY experiment derives the  $^1J_{\text{NH}} + ^1D_{\text{NH}}$  value from dephasing of the  $^1\text{H}^{\text{N}}$  signal and is attractive for its simplicity. However, using an analogous encoding in the  $^{15}\text{N}$  dimension, named 2D SE2 J-TROSY, can be equally or more effective for very large systems with tumbling times in excess of 100 ns.<sup>166</sup>

### 3.2. $^{15}\text{N}$ – $^{13}\text{C}'$ and $^1\text{H}^{\text{N}}$ – $^{13}\text{C}'$

Although measured less widely, accurate values for the  $^{15}\text{N}$ – $^{13}\text{C}'$  and  $^1\text{H}^{\text{N}}$ – $^{13}\text{C}'$  backbone amide RDCs often can be obtained with little effort. Owing to their larger internuclear distances and the lower magnetogyric ratio of  $^{13}\text{C}$  compared to  $^1\text{H}$ , these couplings are intrinsically much smaller than the one-bond  $^1\text{H}$ – $^{15}\text{N}$  RDCs (Table 2), but they can easily be

**Table 2.** Ratios,  $\Lambda$ , of Dipolar Couplings Relative to  $^1D_{\text{NH}}$  for Vectors Pointing in the Same Direction

coupling	$\Lambda$
$^1D_{\text{CaHa}}$	−2.06
$^1D_{\text{CaC}'}$	−0.199
$^1D_{\text{NC}'}$	0.120
$^2D_{\text{C}'\text{HN}}$	−0.310
$^1D_{\text{CH}_3^{\alpha}}$	0.628

<sup>a</sup>For the orientation of the symmetry axis.

measured at high precision from simple 2D TROSY-HSQC spectra recorded in the absence of  $^{13}\text{C}'$  decoupling (Figure 6), even for samples with long rotational correlation times.<sup>167</sup> Because the measurement relies on the TROSY effect for  $^{15}\text{N}$  and  $^1\text{H}^{\text{N}}$  line narrowing,<sup>164</sup> results again are best obtained for perdeuterated proteins. When measured with care, such RDCs then fit as well or better than  $^1D_{\text{NH}}$  values to X-ray reference structures.<sup>168</sup> The reason for this better fit is that it is not impacted by small errors in modeling the positions of

hydrogens relative to the carbon and nitrogen backbone atoms of the X-ray coordinates, and owing to the nearly two times larger internuclear separation,  $^2D_{\text{C}'\text{H}}$  is also less sensitive to such errors than  $^1D_{\text{NH}}$ .

### 3.3. $^{13}\text{C}^{\alpha}$ – $^{13}\text{C}'$

The dipolar interaction constant for  $^{13}\text{C}$ – $^{13}\text{C}$  couplings is ca. 5 times lower than that for  $^{15}\text{N}$ – $^1\text{H}$  (Table 2), therefore requiring precise measurement of the couplings to ensure that such RDCs contain meaningful information. For small- and medium-size proteins, the couplings can simply be extracted from HNCO spectra recorded in the absence of  $^{13}\text{C}^{\alpha}$  decoupling during  $^{13}\text{C}'$  evolution. The transverse relaxation rate of  $^{13}\text{C}'$ , and thereby its line width, is dominated by the chemical shift anisotropy (CSA) mechanism, causing this line width to approximately scale with the square of the magnetic field strength. It is therefore preferable to record such spectra at moderate field strengths (500 or 600 MHz  $^1\text{H}$  frequency), where line widths remain relative narrow while affording sufficient S/N and spectral resolution. Whereas for sensitivity optimization the acquisition time durations in the indirect dimensions are commonly limited to  $T_2$  or less, optimal accuracy of measured splittings requires acquisition times that are longer than  $T_2$  in the dimension where the coupling is measured. For  $^{13}\text{C}'$ , optimal acquisition times range from ca. 30 ms for a protein with  $\tau_c \approx 25$  ns to ca. 60 ms for  $\tau_c \approx 10$  ns.  $^{13}\text{C}'$  acquisition times much longer than 60 ms become less effective because long-range  $^{13}\text{C}'$ – $^{13}\text{C}$  couplings then can cause substantial signal loss. If the minimum measurement time for collecting an HNCO spectrum at such high resolution is prohibitive, nonuniform sampling can be used without an increase of the measured peak position uncertainty calculated from eqs 1a and 1b when using a line-shape-enhanced reconstruction algorithm, such as SMILE.<sup>169</sup>

Measurement of  $^{13}\text{C}^{\alpha}$ – $^{13}\text{C}'$  RDCs again is demonstrated for the main protease ( $\text{M}^{\text{Pro}}$ ) of SARS-CoV-2, a 68 kDa homodimer (Figure 7). Well-resolved  $^{13}\text{C}'$ – $^{13}\text{C}^{\alpha}$  splittings in the  $53 \pm 5$  Hz range are observed for all  $^{13}\text{C}'$  resonances, but because the differences between isotropic and aligned splittings are small, adequate digital resolution and the use of suitable peak-picking software are needed to obtain useful data. Residues for which the  $^{13}\text{C}^{\alpha}$ – $^{13}\text{C}'$  RDCs strongly disagree with the X-ray coordinates of this enzyme all fall outside of the regions of well-defined secondary structure (Figure 7).

Measurement of the  $^{13}\text{C}^{\alpha}$ – $^{13}\text{C}'$  RDCs can also be carried out by quantitative  $J$  correlation methods, an approach that can yield higher precision of the extracted couplings per unit of measuring time.<sup>170</sup> Such measurements are carried out using interleaved versions of the HNCO experiment with and without  $^{13}\text{C}'$ – $^{13}\text{C}^{\alpha}$  dephasing during a constant-time  $^{13}\text{C}'$  evolution period. For perdeuterated proteins, even higher precision can be obtained using the HN(CO)CA pulse scheme, which takes advantage of the slow  $^{13}\text{C}^{\alpha}$  transverse relaxation in perdeuterated proteins.<sup>170</sup>

### 3.4. $^{13}\text{C}^{\alpha}$ – $^1\text{H}^{\alpha}$ and $^{13}\text{C}^{\beta}$ – $^1\text{H}^{\beta}$

The  $^{13}\text{C}^{\alpha}$ – $^1\text{H}^{\alpha}$  RDCs typically are the largest one-bond couplings in proteins, but they can be more challenging to measure in all but the smallest proteins because of extensive spectral overlap in the  $^1\text{H}$ – $^{13}\text{C}$  HSQC spectra which, in addition, lose sensitivity when recorded in the higher resolution, constant-time mode. However, because the couplings are intrinsically large, a lower precision in their measurement can be tolerated. In practice, for all but the

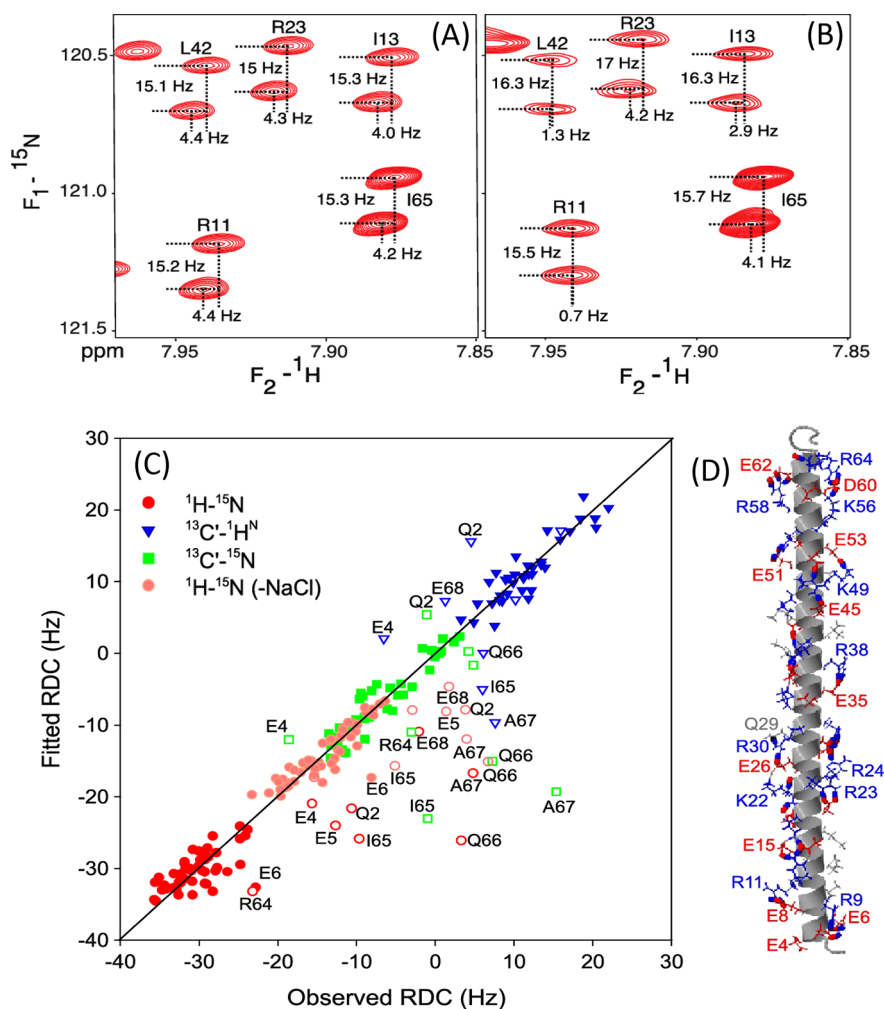


**Figure 6.** RDC measurement and fit of the single  $\alpha$ -helical domain of myosin VI, aligned in 25 mM phosphate buffer, pH 6.3. (A and B) Small region of the 900-MHz  $^{13}\text{C}'$ -coupled 2D  $^1\text{H}$ - $^{15}\text{N}$  TROSY-HSQC spectrum under (A) isotropic and (B) aligned (13 mg/mL Pfl) conditions. Doublets show E.COSY splittings due to  $^1J_{\text{NC}'} + ^1D_{\text{NC}'}$  (vertical) and  $^2J_{\text{HC}'} + ^2D_{\text{HC}'}$  (horizontal). (C) Cross-validated fit of the observed RDCs, normalized by their dipolar interaction constants (Table 2), to the structure. Values for residues near the termini are depicted by open symbols.  $^1D_{\text{NH}}$  couplings on the same sample and at higher salt concentration (salmon) are included for reference. (D) Calculated NMR structure with side chains involved in salt bridge stabilization based on modeling. (Adapted with permission from ref 13. Copyright 2001 American Chemical Society.)

application to residue-specific dynamics analysis, which requires very high precision, a measurement precision that is at least an order of magnitude better than the alignment tensor amplitude,  $D_a$ , expressed in Hertz, more than suffices. Most easily, such couplings are then derived from HN(CO)CA or HNCA triple-resonance spectra, recorded with a relatively short  $^{13}\text{C}^\alpha$  acquisition time of ca. 11 ms and without  $^1\text{H}^\alpha$  decoupling during  $^{13}\text{C}^\alpha$  evolution. Because the signals in such  $^1\text{H}^\alpha$ -coupled spectra consist of two doublet components, the signal-to-noise will be 2-fold lower than that in standard HN(CO)CA or HNCA spectra, and with the doublet components having a large line width of ca. 90 Hz, a high S/N ( $\geq 30:1$ ) is needed to yield sufficient accuracy of the extracted RDCs (cf. eqs 1a and 1b). Typically, the quality of such spectra deteriorates rapidly for  $\tau_c \gtrsim 12$  ns, i.e., proteins or protein complexes larger than ca. 25 kDa, unless they are perdeuterated. However, perdeuteration makes it impossible to measure one-bond  $^{13}\text{C}-^1\text{H}$  RDCs unless  $\text{H}^\alpha$  sites are re protonated.<sup>171,172</sup>

A little used but quite effective method for simultaneous measurement of the  $^{13}\text{C}^\alpha-^1\text{H}^\alpha$  and  $^{13}\text{C}^\beta-^1\text{H}^\beta$  RDCs employs a

slight modification of the fairly sensitive CB(CA)CONH experiment.<sup>173,174</sup> Three such CB(CA)CONH spectra are recorded in an interleaved manner with different durations of  $^1\text{H}$  decoupling during the first, constant-time  $^{13}\text{C}$  evolution period. The relative intensities of the corresponding correlations in the three resulting spectra provide the one-bond  $^{13}\text{C}^\alpha-^1\text{H}^\alpha$  and  $^{13}\text{C}^\beta-^1\text{H}^\beta$  RDCs for residues with a methine  $^{13}\text{C}^\beta$  carbon or the sum of the two  $^{13}\text{C}^\beta-^1\text{H}^\beta$  RDCs for residues with  $^{13}\text{C}^\beta$  methylene carbons.<sup>174</sup>

Measurement of the individual rather than the sum of the  $^{13}\text{C}^\beta-^1\text{H}^\beta$  RDCs of a methylene group is achieved most easily using 75–80% random fractional deuteration and DEPT filtering<sup>175</sup> or other methods<sup>176</sup> to observe exclusively resonances for  $^{13}\text{C}$  with only a single attached proton.<sup>177</sup>

Although RDCs are generally analyzed as orientational restraints relative to a global alignment tensor,  $^{13}\text{C}^\beta-^1\text{H}^\beta$  RDCs can also provide direct local information on the  $\chi_1$  torsion angles provided that the backbone RDCs are also available. This information derives from the observation that, on average,  $\chi_1$  falls within ca.  $8^\circ$  from the ideally staggered states, i.e., the  $t$ ,  $g^+$ , and  $g^-$  rotamers. For example, the  $\text{C}^\beta-^1\text{H}^\beta$

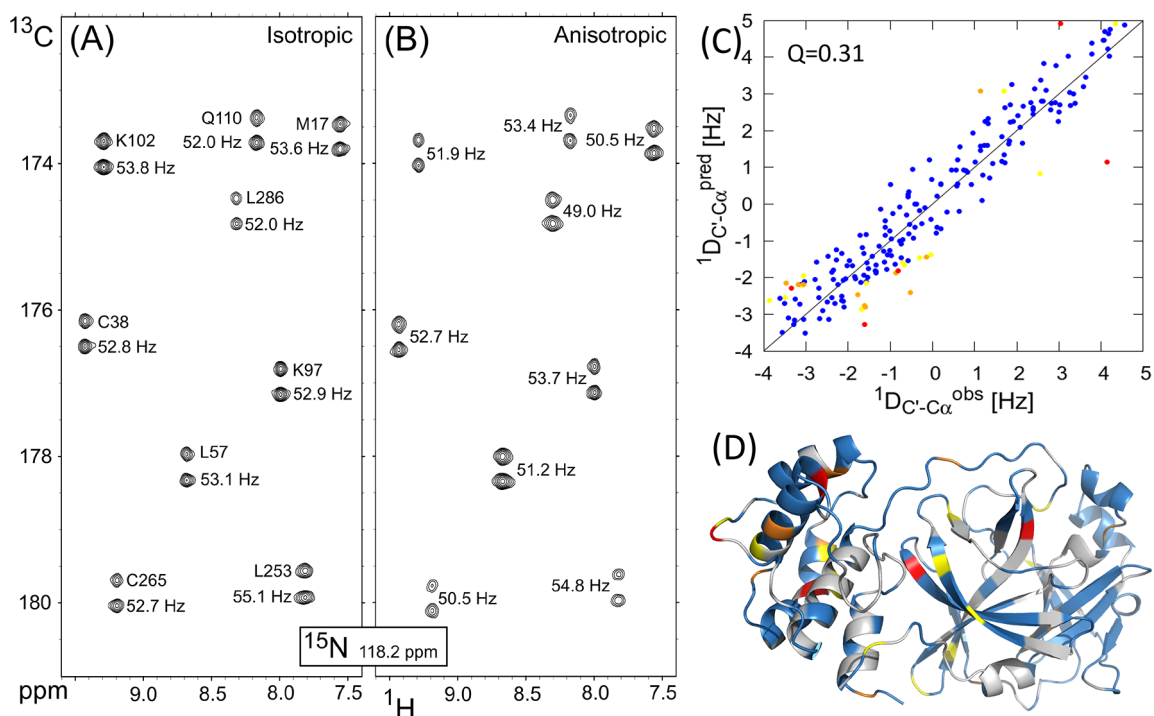


**Figure 7.** Measurement of  $^1D_{C\alpha C'}$  RDCs for the SARS-CoV-2 main protease homodimer from  $^{13}C^{\alpha}$ -coupled 3D TROSY-HNCO spectra recorded at 600 MHz. (A and B)  $^1H$ - $^{13}C'$  cross sections taken orthogonal to the  $^{15}N$  axis at  $\delta(^{15}N) = 118.2$  ppm for (A) the isotropic sample and (B) the sample aligned in 12 mg/mL Pf1. (C) Correlation between observed RDC values and those predicted from the 1.3-Å X-ray structure, PDB entry 5R8T.<sup>14</sup> Only residues with a  $S/N \geq 30:1$  in the aligned spectrum, corresponding to an experimental RDC uncertainty  $\lesssim 1$  Hz, are included in the plot. Symbol colors reflect  $|^1D_{C\alpha C'}^{pred} - ^1D_{C\alpha C'}^{obs}|/TV$  (see eqs 8a and 8b;  $\delta_{\Omega} = 10^{\circ}$ ); ratios  $\leq 1.5$ ,  $1.5$ – $2.0$ ,  $2.0$ – $2.5$ , and  $>2.5$  are shown in blue, yellow, orange, and red, respectively. (D) Ribbon figure of the reference X-ray structure (PDB entry 5R8T), color coded as in C with only the monomeric chain displayed for viewing clarity; residues with a measurement RDC uncertainty  $> 1$  Hz are shown in gray.

bond in Val will be nearly parallel to  $C^{\alpha}$ - $H^{\alpha}$  for the  $t$  conformer but parallel to the  $C^{\alpha}$ - $C'$  or the  $C^{\alpha}$ - $N$  bonds for the  $g^+$  and  $g^-$  rotamers. Because after normalization of the bond lengths and gyromagnetic ratios the RDCs for nearly parallel (or antiparallel) bonds will be roughly the same, simple comparison of the side chain  $C^{\beta}$ - $H^{\beta}$  RDC (or the sum of the two  $C^{\beta}$ - $H^{\beta}$  RDCs for methylene groups) with the backbone RDCs will identify the rotamer state (Figure 8).<sup>177,178</sup> In practice, however, the side chains of many residues rapidly jump back and forth between two or sometimes three

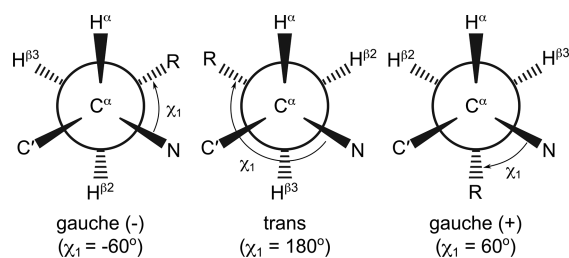


**Figure 8.** Newman projections depicting the three standard  $\chi_1$  rotamers. As can be seen, the different, approximately antiparallel orientations of the side chain  $C^{\beta}$ - $H^{\beta}$  and the backbone  $C^{\alpha}$ - $H^{\alpha}$ ,  $C^{\alpha}$ - $C'$ , and  $C^{\alpha}$ - $N$  vectors that apply for the three canonical rotameric states can be used directly to derive  $\chi_1$  from the corresponding RDC values (after normalization for the different dipolar interaction constants; Table 2), provided  $\chi_1$  does not undergo rapid rotamer averaging. The  $^{13}C^{\alpha}$ - $^{15}N$  RDC is not commonly measured but after normalization, it is close to the  $^{13}C^{\alpha}$ - $^{13}C'$  RDC of the preceding residue.

staggered rotamer states, complicating such analyses<sup>179,180</sup> but often permitting the equilibrium distribution of rotamers to be determined.<sup>176,177</sup>

### 3.5. $^{13}C$ - $^1H$ RDCs in Methyl Groups

Methyl groups have favorable NMR spectroscopic properties: their resonances represent three protons and are correspondingly more intense, and their rapid rotation around their 3-fold symmetry axis reduces the intramethyl group dipolar line broadening. In particular, when used in an otherwise perdeuterated background, methyl signals remain detectable and assignable even for large molecular machines.<sup>181–183</sup> NOE interactions between the methyl groups both aid in the assignment process as well as provide structural information.<sup>184</sup> The RDCs for the methyl groups also are easily measured and can serve as very precise structural reporters. In particular, the RDCs report directly on the orientation of Ala  $C^{\alpha}$ - $C^{\beta}$  bonds and therefore can be used to define relative domain orientations in large protein systems, as highlighted by Prestegard and co-workers for the homodimeric heat-shock protein HtpG.<sup>185</sup>

$^{13}C$ - $^1H$  couplings in methyl groups can be measured by simply removing the  $^1H$  decoupling in the  $^{13}C$  dimension, resulting in a quartet with relative intensities of ca. 3:1:1:3. The outer and more intense quartet components are therefore separated by  $3(^1J_{CH} + ^1D_{CH})$ , which improves the accuracy of the extracted  $^1D_{CH}$  value and compensates for the methyl group rotational scaling factor of  $-0.30$  relative to the RDC of a  $C$ - $H$  bond vector parallel to the symmetry axis of the methyl group.<sup>186</sup> The methyl regions of proteins tend to be crowded, and simply omitting the decoupling increases the number of

resonances 4-fold. However, simple and robust editing can be used to generate spectra that exclusively contain either the most downfield or upfield quartet component, thus simplifying analysis.<sup>187</sup> Alternatively, ultraprecise values can be extracted by fitting the  $J$ -modulation pattern when recording a series of spectra with different  $J$ -dephasing delays.<sup>185</sup>

### 3.6. Oligonucleotides

Nucleic acid structure is known to be sensitive to solvent conditions, and agreement between the structural parameters measured in solution and those predicted by X-ray structures is often much poorer than for proteins, pointing to substantial conformational differences. Because the RDCs are very precise reporters on average bond vector orientations, they are particularly valuable in the study of nucleic acid structure and dynamics.<sup>188</sup> Most commonly measured are the RDCs for  $^{13}\text{C}$ – $^1\text{H}$  correlations of the base and sugar C1'–C4' positions,<sup>189</sup> in addition to those of the imino N–H groups and pyrimidine  $^{13}\text{C5}$ – $^{13}\text{C6}$  couplings. The methods used for their measurement have been reviewed by Getz et al.<sup>190</sup> and in many cases are analogous to those used in proteins with adaptations to minimize the effect of spectral crowding. Similar to proteins, ARTSY measurement of the couplings is a convenient and sensitive method for RDC measurement in nucleic acids, applicable to imino  $^{15}\text{N}$ – $^1\text{H}$  as well as the base C2–H2, C6–H6, and C8–H8 interactions.<sup>191</sup> For small oligonucleotides ( $\lesssim 30$  nucleotides), many two-bond  $^{13}\text{C}$ – $^1\text{H}$  and  $^1\text{H}$ – $^1\text{H}$  couplings are also accessible.<sup>157</sup> However, the richness in spectral information requires particular care during spectral analysis, and these parameters have not yet become widely used in the nucleic acid community.

A new, strikingly simple experiment, demonstrated for the 232-nucleotide HIV-1 Rev response element, is conceptually different from traditional RDC and  $J$ -coupling measurements.<sup>15</sup> This variable flip angle heteronuclear multiple quantum correlation (VF-HMQC) pulse scheme (Figure 9) correlates A-H2 resonances to N1 and N3 via the  $^2J_{\text{NH}} \approx 14.5$  Hz coupling. The measurements are best carried out using oligonucleotides prepared with  $^{15}\text{N}$ -enriched, protonated adenine and perdeuterated U, G, and C nucleotides while using  $\text{D}_2\text{O}$  as the solvent to remove dipolar broadening of H2 by proximate amino and imino protons. For smaller molecules ( $\lesssim 80$  nucleotides), perdeuteration of the nonadenine nucleotides is less important (J. Marchant, personal communication). Adenine H2 resonances remain exceptionally sharp under such conditions, permitting the recording of the two-bond VF-HMQC spectra. Because during the  $\tau \approx 1/(3J) \approx 23$  ms HMQC de- and rephasing delays H2 dephases with respect to both N1 and N3, the H2–N1 correlation intensity depends on  $^2J_{\text{H2N3}}$  and H2–N3 depends on  $^2J_{\text{H2N1}}$ . This dependence on the size of the passive coupling is strongest when  $90^\circ$   $^{15}\text{N}$  pulses are used but modest when using  $45^\circ$   $^{15}\text{N}$  pulses. Therefore, both couplings can be obtained from the ratios of peak intensities recorded with  $45^\circ$  and  $90^\circ$   $^{15}\text{N}$  pulses using the simple relation<sup>15</sup>

$$J_{\text{H2N1}} = \frac{\text{atan}\sqrt{4R_{\text{N3}} - 2}}{\pi\tau} \quad (2)$$

where  $R_{\text{N3}}$  is the intensity ratio observed for the correlation to N3 when using  $45^\circ$  and  $90^\circ$   $^{15}\text{N}$  pulses. Similarly,  $J_{\text{H2N3}}$  is extracted from the intensity ratio observed for the correlation to N1, obtained from the same spectrum. Although the H2–N1/N3 internuclear distances are relatively large (2.06 Å) and

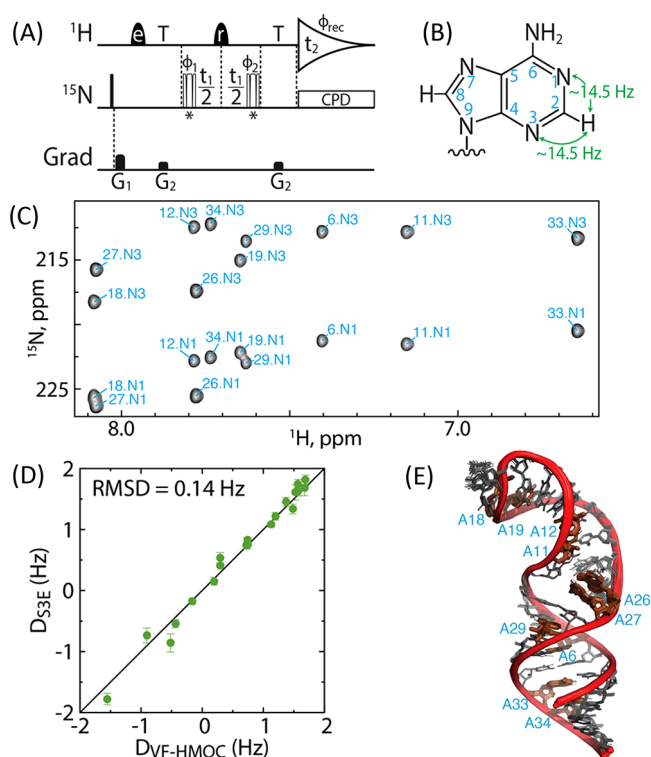


**Figure 9.** High-precision measurement of two-bond H2–N1/N3 RDCs in adenine nucleotides, applicable to large RNAs in  $\text{D}_2\text{O}$ . (A) Pulse sequence of the VF-HMQC experiment. Eburp (e) and Reburp (r) pulses<sup>7</sup> are used for selective excitation of A-H2 resonances, preventing saturation of sugar resonances and thereby permitting a short delay between scans. (B) Two-bond interactions measured by the VF-HMQC. (C) VF-HMQC spectrum recorded for a 36-nt stem-loop RNA construct (E). (D) Comparison of RDC values with those of an  $\text{S}^3\text{E}$  E.COSY experiment. (Adapted with permission from ref 15. Copyright 2001 American Chemical Society.)

the RDCs correspondingly small, the attainable precision is high. Agreement of the RDCs measured in a 36-nt with those of an E.COSY-based measurement was 0.14 Hz with the couplings covering a range of  $\pm 2$  Hz.<sup>15</sup>

## 4. UTILITY OF RDCs IN STRUCTURAL STUDIES

There are three principal applications of RDCs in biomolecular studies: (1) structure calculation and refinement, (2) structure validation, and (3) providing information on dynamics. Whereas 1 and 2 are conceptually quite straightforward, extraction of unique information on the dynamic properties of a biomolecule are intellectually the most interesting and have been comprehensively reviewed by Ruan and Tolman.<sup>6</sup> Here, we limit our discussion to some of the most pertinent, practical aspects of the three areas of RDC applications.

### 4.1. Structure Calculation

For a static structure, the RDCs provide highly sensitive reporters on the orientation of internuclear vectors relative to the alignment tensor of the molecule. The latter is defined by five independent parameters that can be obtained either by an iterative search using the Jacobi method<sup>192</sup> or more efficiently by a singular value decomposition (SVD) best fit of the couplings to the orientations of the vectors in the coordinate frame of the molecule<sup>97,193</sup>

$$D^{AB}(a_x, a_y, a_z) = D_{\text{max}}^{AB} \sum_{i,j=\{x,y,z\}} S_{ij} \cos \alpha_i \cos \alpha_j \quad (3)$$

where  $\cos \alpha_i$  is the direction cosine of the  $A$ – $B$  internuclear vector relative to the  $i$  axis of the molecular coordinate frame and  $D_{\max}^{AB}$  is determined by the internuclear distance,  $r_{AB}$ , and the magnetogyric ratios,  $\gamma$ , of the nuclei involved

$$D_{\max}^{AB} = -\frac{\mu_0 \hbar \gamma_A \gamma_B}{4\pi^2 r_{AB}^3} \quad (4)$$

where  $\hbar$  is Planck's constant divided by  $2\pi$  and  $\mu_0$  is the magnetic permittivity of a vacuum. The  $3 \times 3$  Saupe matrix,  $S$ , is traceless and symmetric. The relation between RDC and vector orientation can be simplified by redefining the molecular coordinate frame such that the Saupe matrix becomes diagonal.<sup>194</sup> In this coordinate frame, the dipolar interaction between two nuclei  $A$  and  $B$  is given by

$$D^{AB}(\theta, \phi) = D_a^{AB}[(3 \cos^2 \theta - 1) + 3/2Rh \sin^2 \theta \cos 2\phi] \quad (5)$$

where  $\theta$  and  $\phi$  are the polar coordinates of the  $A$ – $B$  vector and  $D_a^{AB}$  and  $Rh$  are commonly referred to as the strength and rhombicity of the alignment tensor. As seen from eq 5, the RDC will be at a maximum ( $2D_a^{AB}$ ) if  $A$ – $B$  is aligned parallel to the  $z$  axis of the frame. Inversely, a measured value for the RDC restricts the possible  $A$ – $B$  vector orientations to those of a taco-shaped cone or its inverse (Figure 3).

Deriving the matrix elements  $S_{ij}$  from eq 3 presents a circular problem because a structure is required for the SVD fit. Whereas approximate values for  $D_a^{AB}$  and  $Rh$  can be obtained from a histogram analysis of the measured couplings,<sup>195</sup> a simpler solution is to take advantage of the fact that the alignment tensor enters in linear form in the penalty function that defines the disagreement between the RDCs and the structure. Therefore, the RDCs can be included in the structure calculation procedures while simply leaving the Saupe matrix elements as five adjustable parameters.<sup>149</sup>

As readily seen from symmetry arguments,<sup>25</sup> alignment tensors for oligomeric proteins of  $C_3$  or higher symmetry must be axially symmetric, i.e.,  $Rh = 0$ , with the  $z$  axis of the alignment tensor parallel to the symmetry axis. Similarly, for  $C_2$ -symmetric dimers, one principal axis of the alignment tensor must correspond to the  $C_2$  dimer symmetry axis. Therefore, a minimum of three RDCs per monomer is needed to uniquely define the axially symmetric alignment tensor for a  $C_3$ -symmetric trimer, whereas a minimum of four RDCs is needed for the dimer, and five couplings are needed for a monomeric protein. In practice, however, a 10-fold excess or more of experimental RDCs over the number of fitted parameters is desirable when deriving the 3–5 independent alignment tensor parameters.<sup>196</sup>

## 4.2. Structure Validation

Once the alignment tensor orientation and magnitude have been determined from an SVD fit, the tightness of the correlation between the measured RDCs and the values predicted by the fit can be used to validate the accuracy of the vector orientations in the structural model. This agreement is also impacted by errors in the RDC measurement, but the latter are typically small relative to errors in the structural model (see below).

Thus, the correlation between the experimental RDCs and the corresponding values predicted for the SVD-fitted alignment tensor reports on the consistency between the structural model and the measured RDCs. This agreement is often expressed as a quality factor,  $Q$ <sup>29</sup>

$$Q = \text{rms}(D^{\text{pred}} - D^{\text{meas}}) / \text{rms}(D^{\text{meas}}) \quad (6a)$$

where rms is the root-mean-square function and extends over all of the measured RDCs and  $D^{\text{meas}}$  and  $D^{\text{pred}}$  are the corresponding RDCs predicted when best-fitting the alignment tensor to the coordinates. The RDCs measured for different types of interactions need to be normalized for their dipolar interaction constant,  $\gamma_A \gamma_B / r_{AB}^3$  (cf. Table 2), prior to using eq 6a.

The denominator of eq 6a depends on the orientation of the alignment tensor and will be larger if most internuclear vectors align closely with the  $z$  axis, as observed for the single  $\alpha$ -helical domain of myosin VI.<sup>13</sup> Indeed, the N–H bond vector orientations in many proteins tend to cluster,<sup>197</sup> which impacts the denominator of eq 6a. This dependency can be removed by replacing it by the expected root-mean-square (rms) value of the predicted RDC values as if the vector orientations were randomly distributed<sup>38</sup>

$$Q = \text{rms}(D^{\text{pred}} - D^{\text{meas}}) / \{D_a^2(4 + 3Rh^2)/5\}^{1/2} \quad (6b)$$

We note that an alternate parameter,  $R_{\text{dip}}$ , is sometimes used to express this agreement between dipolar couplings and structural coordinates, where  $R_{\text{dip}} = Q/\sqrt{2}$ .<sup>38</sup>

Clearly, use of  $Q$  or  $R_{\text{dip}}$  as a measure for structural quality is only valid if the RDCs are not used for refinement of the structure. Analogous to the use of the free  $R$  factor in X-ray crystallography,<sup>198</sup> eq 6b therefore must be applied to a small subset of couplings (e.g., 10%) that is randomly omitted from the structure calculation with the calculation repeated many times, each time omitting a different fraction.<sup>38</sup> When deriving such a  $Q_{\text{free}}$  value, care needs to be taken to simultaneously exclude pairs of RDCs for vectors that are approximately parallel due to covalent restraints, such as  $^{15}\text{N}$ – $^{13}\text{C}^\alpha$  of residue  $i$  and  $^{13}\text{C}^\alpha$ – $^{13}\text{C}'$  of residue  $i - 1$ . On the other hand, when multiple types of RDCs are measured, e.g.,  $^{15}\text{N}$ – $^1\text{H}$  and  $^{13}\text{C}'$ – $^{13}\text{C}^\alpha$  or  $^{13}\text{C}^\alpha$ – $^{13}\text{C}^\beta$ , one of these sets may be omitted from the structure calculations and used for structure validation instead. When measuring the same type of coupling in multiple alignment media, which generally will not correspond to orthogonal alignment orientations in the five-dimensional Saupe space,<sup>97</sup> bond vectors used for cross validation should not have input restraints from any of the different media. This latter requirement could be lifted if the experimental RDCs are first “orthogonalized”, i.e., are rearranged as linear combinations that correspond to orthogonal alignment tensors in the five-dimensional Saupe space.<sup>199</sup> Although potentially useful, such orthogonalization is rarely done.

**4.2.1. Impact of Structural Noise.** The steep dependence of the RDC on the orientation of an internuclear vector is both a virtue and a vice. Even very small variations in the bond orientations can give rise to relatively large changes in the predicted RDC. However, the magnitude of the change will depend on the direction in which the bond angle differs. As depicted in Figure 3, a change in orientation that keeps the vector on the rim of the cone leaves the predicted RDCs unchanged, whereas the RDCs are maximally sensitive to changes in the orthogonal orientation. Even there, the predicted RDCs are more sensitive to changes in orientation when values are near zero than when approaching the extreme ends of the RDC range, i.e., close to any of the principal axes of the diagonalized alignment tensor frame where the derivative of eq 5 with respect to  $\theta$  and  $\phi$  is zero

$$\begin{aligned} d(D^{AB}(\theta, \phi))/d\theta \\ = D_a^{AB}[-3 \sin(2\theta) + 3/2Rh \sin(2\theta)\cos(2\phi)] \end{aligned} \quad (7a)$$

$$d(D^{AB}(\theta, \phi))/d\phi = -D_a^{AB}[3Rh \sin^2 \theta \sin(2\phi)] \quad (7b)$$

In practice, this differential dependence of the derivative of the RDC with respect to orientation is large. The agreement between the observed RDCs and the values predicted by a structure therefore is impacted by both the experimental measurement error in the RDC and the uncertainty in the orientation of the internuclear vector. The latter is known as “structural noise” and can result in a small systematic underestimate in the magnitude,  $D_a$ , when using SVD to determine the alignment tensor.<sup>196</sup> When evaluating outliers in the correlation between the measured RDCs and the values predicted by a structural model, both sources of error need to be considered, and only those that exceed a threshold value,  $TV$ , are unambiguous indicators of errors in the model

$$TV = \{(\sigma_D^2 + \sigma_o^2 \delta_\Omega^2)/2\}^{1/2} \quad (8a)$$

where  $\sigma_D$  is the measurement uncertainty,  $\delta_\Omega$  represents the angular uncertainty in internuclear vector orientation, typically ca.  $5^\circ$  for a high-quality X-ray structure solved at a resolution of  $\leq 2 \text{ \AA}$ , and  $\sigma_o$  represents the sensitivity to structural noise

$$\begin{aligned} \sigma_o = D_a^{AB} \{ [-3 \sin(2\theta) + 3/2Rh \sin(2\theta)\cos(2\phi)]^2 \\ + [3Rh \sin \theta \sin(2\phi)]^2 \}^{1/2} \end{aligned} \quad (8b)$$

For reference, 15 X-ray structures of ubiquitin solved at a resolution  $\leq 1.8 \text{ \AA}$  (see Supporting Information of Maltsev et al.<sup>86</sup>) have a pairwise rmsd of  $7.7^\circ$  for 65 of its  $^{13}\text{C}'-^{13}\text{C}^\alpha$  vectors and  $9.6^\circ$  for the corresponding backbone N–H vectors. Note that the latter uncertainty is somewhat elevated relative to those of the backbone  $^{15}\text{N}-^{13}\text{C}'$  and  $^{13}\text{C}^\alpha-^{13}\text{C}'$  bonds because the  $^1\text{H}$  positions typically are added by modeling, and some routines (e.g., MOLMOL,<sup>200</sup> DC,<sup>201</sup> and XPLOR-NIH<sup>202</sup>) yield orientations that better agree with the experimental RDCs than others (e.g., Molprobit).<sup>203</sup>

Hence, disagreements between a structural model and experimental RDCs must be interpreted with caution, and only if the discrepancy between the experimental and the predicted RDC significantly exceeds the  $TV$  value of eq 8a can the absence of agreement be interpreted in terms of a structural difference.

**4.2.2. Impact of Internal Motion.** All of the above discussions apply to static structural models, but the RDCs are defined by the orientations of internuclear vectors in the molecular frame and therefore subject to motions that range from very fast bond librations and vibrations to larger amplitude dynamics on slower time scales. Such internal motions are of fundamental importance to protein function, enzyme catalysis and allosteric regulation to name just two. Nuclear spin relaxation is impacted by such motions and has long been used for extracting quantitative information on the time scale and amplitude of internal motions in proteins and nucleic acids.<sup>204–206</sup> Motions are often categorized as fast or slow, where fast refers to processes faster than the rotational correlation time of the molecule. Motions on the fast time scale impact longitudinal ( $R_1$ ) and transverse ( $R_2$ ) relaxation rates as well as the heteronuclear NOE. They are often characterized by a generalized Lipari–Szabo order parameter,  $S^2$ , and a time scale of internal motion,  $\tau_m$ . Slower time scale

motions do not significantly impact  $R_1$ , but they can impact  $R_2$  if the nuclei involved in the motional process change their chemical shift between the different conformational substates in a process commonly referred to as exchange broadening. In favorable cases, exchange between metastable substates can be modeled quantitatively using relaxation dispersion methods in combination with chemical shift information on the substates involved.<sup>207,208</sup>

As will be discussed in section 4.2, the RDCs offer an important complement to relaxation measurements because they can inform on the direction of motions. However, under the assumption that motions can be represented by diffusion in a cone with semiangle  $\beta$ , the impact of motions on the RDCs tends to be small and corresponds to a scaling factor  $S$ , i.e., the square root of the generalized order parameter  $S^2$  used in Lipari–Szabo analysis of relaxation data<sup>204</sup>

$$S = 0.5 \cos \beta (1 + \cos \beta) \quad (9)$$

Relaxation analysis of many globular proteins indicates that, with the exception of N- and C-terminal regions or long intrinsically disordered linker regions,  $S^2$  values for N–H vectors rarely fall outside of the 0.6–0.95 range. Therefore, the  $S$  values mostly cover a relatively narrow range of 0.77–0.98, and use of a uniform value for  $S$  does not introduce large errors in the analysis of globular proteins. Relaxation-derived  $S^2$  values do not include the effect of motions on time scales slower than  $\tau_c$ , but in a small globular protein for which very high quality data were collected, such slower motions proved to be the exception rather than the rule.<sup>103,209</sup>

The above arguments suggest that exclusion of the RDCs from residues in short loops and turns because of possibly increased dynamics is ill advised. Frequently, poor fits between the RDCs and the structural coordinates for such residues result from either true structural differences between solution and the crystalline state or difficulties in accurately modeling such regions. In the solution NMR structures derived from the NOE data, fewer well-defined restraints are typically available for such loop and turn regions, also contributing to below average validation statistics.

### 4.3. Extracting Dynamics from the RDCs

Two types of motions must be distinguished: those that impact the alignment tensor and those that do not. Changes in the average molecular orientation resulting from the forces that generate alignment cannot occur on a time scale faster than  $\tau_c$ , and fast motions therefore can only impact the average alignment but do not make it time dependent. At the other end of the spectrum there are slow conformational changes, for example, associated with ligand binding, allosteric activation, or dynamic switching between open and closed states. These latter types of motions are often more difficult to tackle but arguably also more interesting. As discussed below, RDCs offer powerful avenues to study both types of dynamic processes.

**4.3.1. Motions That Do Not Impact Molecular Alignment.** As discussed above, under the diffusion-in-a-cone model, the impact of intramolecular motions is generally small. Relaxation analysis is generally unable to distinguish details of rapid dynamic processes other than their amplitude and their time scale. RDCs can provide access to time scales when processes are slow,<sup>210</sup> but this requires exceptionally precise measurements. More importantly, RDCs contain information on the direction in which motions take place. Visually, this is easily appreciated by considering the vector

orientation mapped in Figure 3. Oscillations around an equilibrium orientation that keep the vector on the black cone have no impact on the magnitude of the RDC, whereas excursions in the orthogonal direction strongly modulate the RDC and usually decrease its absolute value. If the RDCs are measured under a second alignment condition, where values on the blue cone in Figure 3 correspond to the measured RDC value, the effect of motion is the opposite: motions that leave the RDC unchanged under the black cone alignment condition have a maximum impact on those in the medium that gives rise to the blue cone.

Both the amplitudes and the directions of the internuclear vector motions can be extracted from RDC data provided that high-quality measurements are available under five orthogonal alignment conditions.<sup>4–6</sup> The latter requirement can be challenging because molecular alignment is dominated by steric and electrostatic interactions, making it difficult to generate five linearly independent alignment conditions, as assessed quantitatively by SECONDA analysis.<sup>211</sup> Note that conventional, three-dimensional spatial intuition is not particularly helpful in guiding the selection of mutants needed to generate five orthogonal alignment conditions of the type depicted in Figure 2. Conservative mutations of charges on the protein's surface can also be used to alter its alignment, but it generally is challenging to predict which mutations will optimally span the five-dimensional alignment space without impacting the protein backbone structure.<sup>212</sup> Implementation of the paramagnetically tagged GB3 domain strategy,<sup>103</sup> where the mutants that yield sufficient variation in alignment already have been designed, circumvents this otherwise challenging design question.

**4.3.2. Motions That Impact the Alignment.** When intramolecular motions significantly impact the alignment tensor, the simple description of eq 3 no longer applies. As each conformer has its own alignment tensor, defined by five parameters, determination of a unique ensemble that fits the RDCs rapidly becomes an intractable problem unless prior information on the alignment of individual substates is known.<sup>12</sup> For the hemagglutinin fusion peptide, a tight helical hairpin structure was found at neutral pH based on a very large set of RDCs and NOEs,<sup>213</sup> but at lower pH some exchange broadening and chemical shift changes pointed to transient opening of the helical hairpin. Knowing from chemical shift analysis that upon transient opening of the hairpin the helical secondary structure of its two arms remained intact, the RDCs allowed modeling of the low-pH structure as the rapid average of at least three quite different states: hairpin, partially open, and wide open (Figure 10).<sup>12</sup>

A remarkable example of the application of RDCs to the study of motion in nucleic acids focused on the dynamics introduced by a trinucleotide bulge in a double-stranded RNA helix. After extending the oligomer alternately in the 3' and 5' directions, such that either the far longer 3'-stem or 5'-stem dominates the alignment tensor, the RDCs were used to map both the relative twisting and bending motions of the two A-form helical segments in exquisite detail.<sup>214</sup>

Another important application of RDCs to the study of extremely dynamic systems concerns denatured or intrinsically disordered proteins. For such systems, the alignment for each conformer may be predicted based on a steric occlusion model,<sup>109</sup> an approach successfully used for the study of conformational ensembles of unfolded proteins.<sup>215–217</sup> We note, however, that such ensemble models tend to be

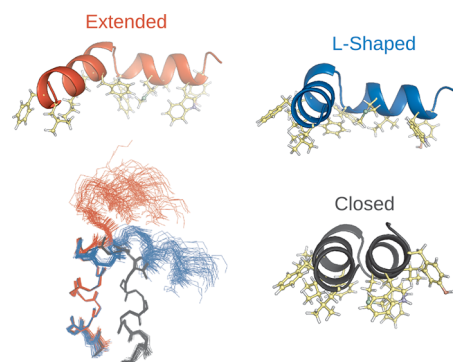


**Figure 10.** Ensemble model for the G8A mutant of the hemagglutinin N-terminal 23-residue fusion peptide, derived from RDCs. Through relaxation and chemical shift measurements, this G8A structure was linked to the wild-type structure at low pH, where membrane fusion occurs. The ensemble model reflects the smaller degrees of alignment experienced by the C-terminal compared to the N-terminal helix. A small population ( $14 \pm 4\%$ ) of the wild-type pH 7 hairpin structure (black) transiently remains present in the G8A mutant. A minimum of two other states (extended and L shaped) is required to fit the RDC data. (Adapted with permission from ref 12. Copyright 2012 National Academy of Sciences of the United States of America.)

underdetermined and in general are unable to identify the presence of small populations of transiently well-ordered conformers unless prior or additional information on the transiently ordered state is available. On the other hand, the transient presence of helical segments can be quite evident from RDC data but is then also reflected in the secondary  $^{13}\text{C}^{\alpha}$  chemical shifts.<sup>218</sup>

**4.3.3. Domain Motions in Paramagnetically Aligned Systems.** Paramagnetic alignment offers a unique tool for studying global structural rearrangements. As first demonstrated by Bertini and co-workers in the classic study of calmodulin,<sup>11</sup> if the aligning force applies to a single domain, the reduction in alignment of other domains can readily be assessed from their alignment tensors (Figure 11). In the calmodulin example, its N-terminal domain was mutated to enable selective replacement of one of its two  $\text{Ca}^{2+}$  ions by either  $\text{Tm}^{3+}$  or  $\text{Tb}^{3+}$  without significantly impacting its structure. Fitting of the N-terminal domain pseudocontact shifts was used to define its alignment tensor for each of the two lanthanides. The reduced alignment of the C-terminal domain relative to the N-terminal domain was then readily ascertained by fitting the measured C-terminal domain RDCs to their known structure, previously refined by RDCs.<sup>219</sup>

The best average alignment of the diamagnetic domain relative to that carrying the lanthanide is obtained by reorienting this domain such that the direct scalar product of the two alignment tensors is maximized. Oscillatory, independent rotations of the diamagnetic domain around each of the principal axes of the alignment tensor of the tagged domain can be defined to generate the requisite scaling, but generation of a realistic motional model generally will be more challenging. For calmodulin, paramagnetic shifts observed for the C-terminal domain resonances represent strong additional constraints on the distances of these nuclei from the lanthanide, and they further restrained the conformational space sampled by this domain.<sup>11</sup> Analysis of a grid search indicated that a minimum of three distinctly different C-terminal domain orientations was needed to adequately fit the PCS and RDC data.

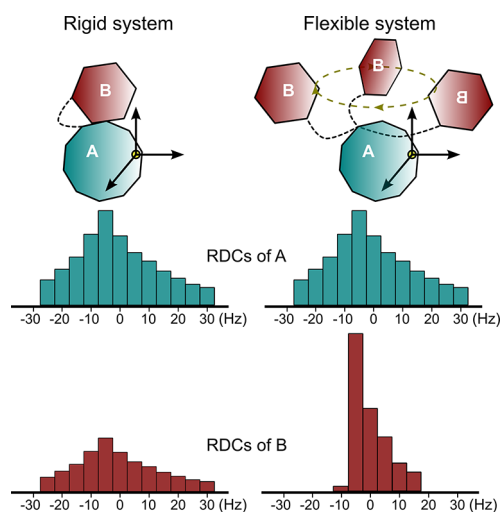


**Figure 11.** Schematic effect of motion on the RDCs in a two-domain protein, where alignment of domain A, marked by the axis system, is caused by tight binding of a paramagnetic lanthanide ion to this domain. For a rigidly linked system (left), the RDCs for domain B span the same range as domain A. For a flexibly linked system (right), alignment of B is reduced. Reduction in alignment of B relative to A together with PCS can be used to generate a quantitative motional model for the interdomain motion.<sup>11</sup>

Another conceptually simpler example of lanthanide alignment to study molecular flexibility concerns the single  $\alpha$ -helical (SAH) domain of myosin VI.<sup>13</sup> Such SAH domains are fairly abundant in mammalian proteins and have been proposed to function as lever arm extensions in several members of the myosin protein family.<sup>220</sup> Whereas most  $\alpha$ -helices require tertiary interactions for stabilization and are only metastable when studied as isolated peptides, SAH domains form stable helical structures in isolation. They consist of repeats of 4-residue acidic (mostly Glu) and basic (mostly Lys and Arg) segments with dynamic salt bridges between residues spaced one helical turn apart stabilizing such helices.<sup>221</sup> The question of whether the finite persistence length of such helices is caused by transient breaks at spots where the sequence deviates from the canonical repeat pattern or simply results from small backbone torsion angle fluctuations without requiring such breaks has been answered by paramagnetic alignment. By tagging the SAH domain of myosin VI near its N-terminus with a M8Spy-Tm tag, the helix becomes locally aligned with respect to the magnetic field, presumably strongest at the site of the tagged residue, Cys-13. Whereas the amides of residues 3–23 in the SAH domain vanished due to paramagnetic broadening, residues 24–65 show a monotonic exponential decay of the  $\alpha$ -helical oscillatory dipolar wave pattern<sup>8</sup> and thus a monotonic decrease in alignment (Figure 12).<sup>13</sup> This result shows that at room temperature this SAH domain behaves like a uniformly flexible rod, with a persistence length of  $224 \pm 10$  Å, without any evidence of “soft spots” or kinks.

## 5. CONCLUDING REMARKS AND OUTLOOK

Key questions regarding signaling across membranes remain at the forefront of molecular and structural biology. Here, the equilibria between multiple states depend on many variables, making such systems very challenging to study by computational or crystallographic methods.<sup>222</sup> Whereas with the introduction of TROSY technology the size of such systems

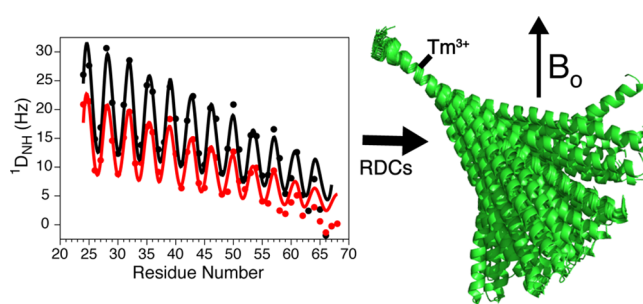


**Figure 12.** Decrease in the  $^1D_{\text{NH}}$  RDCs measured for the single  $\alpha$ -helical domain of myosin-VI with increasing distance from the site of attachment (Cys-13) of a M8Spy-Tm<sup>3+</sup> paramagnetic tag.  $^1D_{\text{NH}}$  RDCs measured at 20 (black) and 35 °C (red) both show the “dipolar wave” oscillation, characteristic of an  $\alpha$ -helix.<sup>8</sup> Decrease in amplitude of both the dipolar wave oscillations and the average RDC was fitted to helix persistence lengths of 224 (20 °C) and 165 Å (35 °C), giving rise to a dynamic ensemble of conformations as schematically depicted by the green helices. (Reprinted with permission from ref 13. Copyright 2019 American Chemical Society.)

is no longer prohibitive for NMR studies,<sup>223</sup> interpretation of chemical shift changes associated with different structural substates remains difficult. RDC measurements on such systems have remained challenging too, mostly because generating robust liquid crystalline media for aligning very large protein–lipid aggregates has remained difficult, and the use of acrylamide gels decreases their rates of rotational diffusion and thereby their spectral resolution. Although direct paramagnetic tagging at a solvent-accessible site of such systems is feasible,<sup>137</sup> flexibility of the tag can reduce alignment of the protein to below optimal levels. Paramagnetic tagging with a bulky, tagged domain<sup>103</sup> will mitigate this problem and may therefore further facilitate exploitation of the unambiguous and precise information contained in the RDCs.

Many of the early applications of protein and nucleic acid NMR focused on determination of atomic resolution structural models,<sup>24</sup> frequently a labor-intensive and time-consuming endeavor. Perhaps disappointing, for cases where both NMR-derived and X-ray structures are available, the X-ray models frequently fit better to the RDCs than structures obtained from solution NMR data, highlighting the difficulties in refining such structures to the level of high-resolution crystal structures. Moreover, recent computational methods have been shown to be capable of generating high-quality structural models in silico.<sup>153,154</sup> In particular, the emergence of AlphaFold2<sup>155</sup> appears to relegate much of the conventional NMR structure determination endeavors to the sidelines. However, this development potentially is very favorable for biological NMR because it allows the technology to focus on the more interesting mechanistic questions. These frequently involve structural rearrangements on a nearly flat energy surface related to folding–unfolding equilibria, binding phenomena, allosteric activation, or dynamic rearrangements that underlie virtually every signaling and regulatory pathway and are often at the heart of enzyme reaction mechanisms. RDCs are invaluable in such studies as they directly report on such structural rearrangements at the high precision required to relate the structure, function, and related global dynamic processes.

Whereas RDCs place tight structural restraints on the orientations of bond vectors as well as entire well-defined structural domains, they do not contain translational

information. For this reason, other NMR parameters such as those derived from paramagnetic relaxation enhancement (PRE)<sup>45,104,224,225</sup> and pseudocontact shifts (PCS)<sup>226,142</sup> that do define long-range distances are an invaluable complement to the RDCs.<sup>225–227</sup> Similarly, shape information derived from small-angle X-ray scattering (SAXS) can provide another powerful complement to RDCs.<sup>45</sup>

## AUTHOR INFORMATION

### Corresponding Author

**Ad Bax** – Laboratory of Chemical Physics, National Institute of Diabetes and Digestive and Kidney Diseases, National Institutes of Health, Bethesda, Maryland 20892, United States; [orcid.org/0000-0002-9809-5700](https://orcid.org/0000-0002-9809-5700); Email: [bax@nih.gov](mailto:bax@nih.gov)

### Authors

**Sai Chaitanya Chiliveri** – Laboratory of Chemical Physics, National Institute of Diabetes and Digestive and Kidney Diseases, National Institutes of Health, Bethesda, Maryland 20892, United States

**Angus J. Robertson** – Laboratory of Chemical Physics, National Institute of Diabetes and Digestive and Kidney Diseases, National Institutes of Health, Bethesda, Maryland 20892, United States

**Yang Shen** – Laboratory of Chemical Physics, National Institute of Diabetes and Digestive and Kidney Diseases, National Institutes of Health, Bethesda, Maryland 20892, United States

**Dennis A. Torchia** – Laboratory of Chemical Physics, National Institute of Diabetes and Digestive and Kidney Diseases, National Institutes of Health, Bethesda, Maryland 20892, United States

Complete contact information is available at:  
<https://pubs.acs.org/10.1021/acs.chemrev.1c00730>

### Notes

The authors declare no competing financial interest.

### Biographies

Sai Chaitanya Chiliveri received his Ph.D. degree in Biophysics under the supervision of Dr. Mandar V. Deshmukh at the Centre for Cellular and Molecular Biology, India, in 2016. His research focused on understanding the functional diversity of dsRNA binding proteins in the RNA interference pathway of *C. elegans* and *A. thaliana*. In 2016, he joined the group headed by Ad Bax at the National Institutes of Health as a postdoctoral fellow, where he currently employs solution NMR methods to investigate the molecular details of membrane fusion between enveloped viruses and host cells, mediated by the spike proteins of HIV-1 and SARS-CoV-2. His research interests include host–pathogen interactions, biomolecular NMR spectroscopy, and structural biology of membrane-associated proteins.

Angus J. Robertson is a postdoctoral researcher in the Bax group at NIH/NIDDK. He obtained his Ph.D. degree in Biomolecular NMR under the supervision of Prof. Jonathan Waltho at the University of Sheffield, U.K., where he investigated transition-state analogues of phosphoryl transfer reactions. His current research interests involve development of novel NMR methodologies such as pressure-jump NMR to characterize aggregating systems as well mechanistic investigation of challenging enzyme systems like the main protease of SARS-CoV-2.

Yang Shen is a Staff Scientist in the Laboratory of Chemical Physics, National Institute of Diabetes and Digestive and Kidney Diseases (LCP/NIDDK). Before his current academic position, he received his Ph.D. degree from the State University of New York at Buffalo and worked as a postdoctoral research fellow with Dr. Ad Bax at LCP/NIDDK. His research interests focus on developing NMR-based computational methods and user-friendly software including the widely used SPARTA, TALOS+/TALOS-N, POMONA, CS-ROSETTA, and other programs.

Dennis Torchia is an American biophysicist who extensively used NMR spectroscopy to study protein dynamics and structure in order to better understand function. He spent most of his career at the National Institute of Dental and Craniofacial Research (NIDCR), where he served as Chief of the Structural Biology Unit before his retirement in 2006. He remains active as a special volunteer at the National Institute of Diabetes and Digestive and Kidney Diseases at the NIH.

Ad Bax was trained in Applied Physics and Physical Chemistry at Delft University of Technology, The Netherlands, supervised by Toon Mehlkopf and in the research group of Ray Freeman at Oxford University, England, where he gained his passion for NMR spectroscopy. After a postdoctoral stint with Gary Maciel at the National High Field Solid-State NMR Center in Ft. Collins, CO, he joined the National Institutes of Health in 1983, where he currently is Chief of the Section on Biophysical NMR Spectroscopy in the Laboratory of Chemical Physics at the National Institute of Diabetes and Digestive and Kidney Diseases.

## ACKNOWLEDGMENTS

This work was supported by the Intramural Program of the National Institute of Diabetes and Digestive and Kidney Diseases, NIH.

## REFERENCES

- (1) Schmidt, J. M.; Howard, M. J.; Maestre-Martinez, M.; Perez, C. S.; Loehr, F. Variation in protein C-alpha-related one-bond J couplings. *Magn. Reson. Chem.* **2009**, *47*, 16–30.
- (2) Wienk, H. L. J.; Martinez, M. M.; Yalloway, G. N.; Schmidt, J. M.; Pérez, C.; Rüterjans, H.; Löhr, F. Simultaneous measurement of protein one-bond and two-bond nitrogen-carbon coupling constants using an internally referenced quantitative J-correlated [15N,1H]-TROSY-HNC experiment. *J. Biomol. NMR* **2003**, *25*, 133–145.
- (3) Schmidt, J. M.; Zhou, S.; Rowe, M. L.; Howard, M. J.; Williamson, R. A.; Löhr, F. One-bond and two-bond J couplings help annotate protein secondary-structure motifs: J-coupling indexing applied to human endoplasmic reticulum protein ERp18. *Proteins: Struct., Funct., Genet.* **2011**, *79*, 428–443.
- (4) Peti, W.; Meiler, J.; Bruschweiler, R.; Griesinger, C. Model-free analysis of protein backbone motion from residual dipolar couplings. *J. Am. Chem. Soc.* **2002**, *124*, 5822–5833.
- (5) Lange, O. F.; Lakomek, N. A.; Fares, C.; Schroder, G. F.; Walter, K. F. A.; Becker, S.; Meiler, J.; Grubmüller, H.; Griesinger, C.; de Groot, B. L. Recognition dynamics up to microseconds revealed from an RDC-derived ubiquitin ensemble in solution. *Science* **2008**, *320*, 1471–1475.
- (6) Tolman, J. R.; Ruan, K. NMR residual dipolar couplings as probes of biomolecular dynamics. *Chem. Rev.* **2006**, *106*, 1720–1736.
- (7) Geen, H.; Freeman, R. Band-selective radiofrequency pulses. *J. Magn. Reson.* **1991**, *93*, 93–141.
- (8) Mesleh, M. F.; Opella, S. J. Dipolar Waves as NMR maps of helices in proteins. *J. Magn. Reson.* **2003**, *163*, 288–299.
- (9) Fitzkee, N. C.; Bax, A. Facile measurement of H-1-N-15 residual dipolar couplings in larger perdeuterated proteins. *J. Biomol. NMR* **2010**, *48*, 65–70.

- (10) Gaemers, S.; Bax, A. Morphology of three lyotropic liquid crystalline biological NMR media studied by translational diffusion anisotropy. *J. Am. Chem. Soc.* **2001**, *123*, 12343–12352.
- (11) Bertini, I.; Del Bianco, C.; Gelis, L.; Katsaros, N.; Luchinat, C.; Parigi, G.; Peana, M.; Provenzani, A.; Zoroddu, M. A. Experimentally exploring the conformational space sampled by domain reorientation in calmodulin. *Proc. Natl. Acad. Sci. U. S. A.* **2004**, *101*, 6841–6846.
- (12) Lorieau, J. L.; Louis, J. M.; Schwieters, C. D.; Bax, A. pH-triggered, activated-state conformations of the influenza hemagglutinin fusion peptide revealed by NMR. *Proc. Natl. Acad. Sci. U. S. A.* **2012**, *109*, 19994–19999.
- (13) Barnes, C. A.; Shen, Y.; Ying, J. F.; Takagi, Y.; Torchia, D. A.; Sellers, J. R.; Bax, A. Remarkable rigidity of the single alpha-helical domain of myosin-VI as revealed by NMR spectroscopy. *J. Am. Chem. Soc.* **2019**, *141*, 9004–9017.
- (14) Douangamath, A.; Fearon, D.; Gehrtz, P.; Krojer, T.; Lukacik, P.; Owen, C. D.; Resnick, E.; Strain-Damerell, C.; Aimon, A.; Abranyi-Balogh, P.; et al. Crystallographic and electrophilic fragment screening of the SARS-CoV-2 main protease. *Nat. Commun.* **2020**, *11*, 5047.
- (15) Marchant, J.; Bax, A.; Summers, M. F. Accurate measurement of residual dipolar couplings in large RNAs by variable flip angle NMR. *J. Am. Chem. Soc.* **2018**, *140*, 6978–6983.
- (16) Vuister, G. W.; Boelens, R.; Kaptein, R. Non-selective 3-dimensional NMR spectroscopy - The 3D NOE-HOHAHA experiment. *J. Magn. Reson.* **1988**, *80*, 176–185.
- (17) Wagner, G.; Hyberts, S. G.; Havel, T. F. NMR structure determination in solution - A critique and comparison with X-ray crystallography. *Annu. Rev. Biophys. Biomol. Struct.* **1992**, *21*, 167–198.
- (18) Kay, L. E.; Clore, G. M.; Bax, A.; Gronenborn, A. M. Four-dimensional heteronuclear triple-resonance NMR spectroscopy of interleukin-1B in solution. *Science* **1990**, *249*, 411–414.
- (19) Hiller, S.; Fiorito, F.; Wuthrich, K.; Wider, G. Automated projection spectroscopy (APSY). *Proc. Natl. Acad. Sci. U. S. A.* **2005**, *102*, 10876–10881.
- (20) Bax, A.; Grzesiek, S. Methodological advances in protein NMR. *Acc. Chem. Res.* **1993**, *26*, 131–138.
- (21) Wishart, D. S.; Sykes, B. D. Chemical shifts as a tool for structure determination. *Methods Enzymol.* **1994**, *239*, 363–392.
- (22) Pardi, A.; Billeter, M.; Wüthrich, K. Calibration of the angular dependence of the amide proton- $\alpha$  proton coupling constants,  $^3J_{\text{HNH}}$ , in a globular protein: Use of  $^3J_{\text{HNH}}$  for identification of helical secondary structure. *J. Mol. Biol.* **1984**, *180*, 741–751.
- (23) Wang, A. C.; Bax, A. Determination of the backbone dihedral angles phi in human ubiquitin from reparametrized empirical Karplus equations. *J. Am. Chem. Soc.* **1996**, *118*, 2483–2494.
- (24) Wüthrich, K. *NMR of Proteins and Nucleic Acids*; John Wiley & Sons: New York, 1986.
- (25) Prestegard, J. H.; Al-Hashimi, H. M.; Tolman, J. R. NMR structures of biomolecules using field oriented media and residual dipolar couplings. *Q. Rev. Biophys.* **2000**, *33*, 371–424.
- (26) Blackledge, M. Recent progress in the study of biomolecular structure and dynamics in solution from residual dipolar couplings. *Prog. Nucl. Magn. Reson. Spectrosc.* **2005**, *46*, 23–61.
- (27) Bax, A. Weak alignment offers new NMR opportunities to study protein structure and dynamics. *Protein Sci.* **2003**, *12*, 1–16.
- (28) Chen, K.; Tjandra, N., The Use of Residual Dipolar Coupling in Studying Proteins by NMR. In *NMR of Proteins and Small Biomolecules*; Zhu, G., Ed.; Springer, 2012; Vol. 326, pp 47–67.
- (29) Cornilescu, G.; Marquardt, J. L.; Ottiger, M.; Bax, A. Validation of protein structure from anisotropic carbonyl chemical shifts in a dilute liquid crystalline phase. *J. Am. Chem. Soc.* **1998**, *120*, 6836–6837.
- (30) Hallwass, F.; Schmidt, M.; Sun, H.; Mazur, A.; Kummerlowe, G.; Luy, B.; Navarro-Vazquez, A.; Griesinger, C.; Reinscheid, U. M. Residual Chemical Shift Anisotropy (RCSA): A Tool for the Analysis of the Configuration of Small Molecules. *Angew. Chem., Int. Ed.* **2011**, *50*, 9487–9490.
- (31) Liu, Y.; Sauri, J.; Mevers, E.; Pecuh, M. W.; Hiemstra, H.; Clardy, J.; Martin, G. E.; Williamson, R. T. Unequivocal determination of complex molecular structures using anisotropic NMR measurements. *Science* **2017**, *356*, aam5349.
- (32) Nath, N.; Schmidt, M.; Gil, R. R.; Williamson, R. T.; Martin, G. E.; Navarro-Vazquez, A.; Griesinger, C.; Liu, Y. Z. Determination of Relative Configuration from Residual Chemical Shift Anisotropy. *J. Am. Chem. Soc.* **2016**, *138*, 9548–9556.
- (33) Ketchem, R. R.; Lee, K. C.; Huo, S.; Cross, T. A. Macromolecular structural elucidation with solid-state NMR- derived orientational constraints. *J. Biomol. NMR* **1996**, *8*, 1–14.
- (34) Ketchem, R. R.; Hu, W.; Cross, T. A. High-resolution conformation of gramicidin-A in a lipid bilayer by solid-state NMR. *Science* **1993**, *261*, 1457–1460.
- (35) Quine, J. R.; Brenneman, M. T.; Cross, T. A. Protein structural analysis from solid-state NMR-derived orientational constraints. *Biophys. J.* **1997**, *72*, 2342–2348.
- (36) Schwieters, C. D.; Kuszewski, J. J.; Tjandra, N.; Marius Clore, G. The Xplor-NIH NMR molecular structure determination package. *J. Magn. Reson.* **2003**, *160*, 65–73.
- (37) Guntert, P. Automated structure determination from NMR spectra. *Eur. Biophys. J.* **2009**, *38*, 129–143.
- (38) Clore, G. M.; Garrett, D. S. R-factor, free R, and complete cross-validation for dipolar coupling refinement of NMR structures. *J. Am. Chem. Soc.* **1999**, *121*, 9008–9012.
- (39) Ottiger, M.; Bax, A. Bicelle-based liquid crystals for NMR-measurement of dipolar couplings at acidic and basic pH values. *J. Biomol. NMR* **1999**, *13*, 187–191.
- (40) Tolman, J. R. Dipolar couplings as a probe of molecular dynamics and structure in solution. *Curr. Opin. Struct. Biol.* **2001**, *11*, 532–539.
- (41) Bryson, M.; Tian, F.; Prestegard, J. H.; Valafar, H. REDCRAFT: A tool for simultaneous characterization of protein backbone structure and motion from RDC data. *J. Magn. Reson.* **2008**, *191*, 322–334.
- (42) Dosset, P.; Hus, J. C.; Marion, D.; Blackledge, M. A novel interactive tool for rigid-body modeling of multi-domain macromolecules using residual dipolar couplings. *J. Biomol. NMR* **2001**, *20*, 223–231.
- (43) Prestegard, J. H.; Bougault, C. M.; Kishore, A. I. Residual dipolar couplings in structure determination of biomolecules. *Chem. Rev.* **2004**, *104*, 3519–3540.
- (44) Gobl, C.; Madl, T.; Simon, B.; Sattler, M. NMR approaches for structural analysis of multidomain proteins and complexes in solution. *Prog. Nucl. Magn. Reson. Spectrosc.* **2014**, *80*, 26–63.
- (45) Venditti, V.; Egner, T. K.; Clore, G. M. Hybrid approaches to structural characterization of conformational ensembles of complex macromolecular systems combining NMR residual dipolar couplings and solution X-ray scattering. *Chem. Rev.* **2016**, *116*, 6305–6322.
- (46) Tzvetkova, P.; Sternberg, U.; Gloge, T.; Navarro-Vazquez, A.; Luy, B. Configuration determination by residual dipolar couplings: accessing the full conformational space by molecular dynamics with tensorial constraints. *Chemical Science* **2019**, *10*, 8774–8791.
- (47) Liu, Y.; Navarro-Vázquez, A.; Gil, R. R.; Griesinger, C.; Martin, G. E.; Williamson, R. T. Application of anisotropic NMR parameters to the confirmation of molecular structure. *Nat. Protoc.* **2019**, *14*, 217–247.
- (48) Gayathri, C.; Tsarevsky, N. V.; Gil, R. R. Residual dipolar couplings (RDCs) analysis of small molecules made easy: Fast and tuneable alignment by reversible compression/relaxation of reusable PMMA gels. *Chem. - Eur. J.* **2010**, *16*, 3622–3626.
- (49) Verdier, L.; Sakhaii, P.; Zweckstetter, M.; Griesinger, C. Measurement of long range  $H/C$  couplings in natural products in orienting media: a tool for structure elucidation of natural products. *J. Magn. Reson.* **2003**, *163*, 353–359.
- (50) Freudenberg, J. C.; Spittler, P.; Bauer, R.; Kessler, H.; Luy, B. Stretched poly(dimethylsiloxane) gels as NMR alignment media for apolar and weakly polar organic solvents: An ideal tool for

measuring RDCs at low molecular concentrations. *J. Am. Chem. Soc.* **2004**, *126*, 14690–14691.

(51) Freudenberger, J. C.; Knor, S.; Kobzar, K.; Heckmann, D.; Paululat, T.; Kessler, H.; Luy, B. Stretched poly(vinyl acetate) gels as NMR alignment media for the measurement of residual dipolar couplings in polar organic solvents. *Angew. Chem., Int. Ed.* **2005**, *44*, 423–426.

(52) Kummerlowe, G.; Behl, M.; Lendlein, A.; Luy, B. Artifact-free measurement of residual dipolar couplings in DMSO by the use of cross-linked perdeuterated poly(acrylonitrile) as alignment medium. *Chem. Commun. (Cambridge, U. K.)* **2009**, *46*, 8273–8275.

(53) Zong, W.; Li, G. W.; Cao, J. M.; Lei, X. X.; Hu, M. L.; Sun, H.; Griesinger, C.; Tan, R. X. An alignment medium for measuring residual dipolar couplings in pure DMSO: liquid crystals from graphene oxide grafted with polymer brushes. *Angew. Chem., Int. Ed.* **2016**, *55*, 3690–3693.

(54) Lei, X.; Qiu, F.; Sun, H.; Bai, L.; Wang, W.-X.; Xiang, W.; Xiao, H. A self-assembled oligopeptide as a versatile NMR alignment medium for the measurement of residual dipolar couplings in methanol. *Angew. Chem., Int. Ed.* **2017**, *56*, 12857–12861.

(55) Qin, S. Y.; Jiang, Y.; Sun, H.; Liu, H.; Zhang, A. Q.; Lei, X. X. Measurement of residual dipolar couplings of organic molecules in multiple solvent systems using a liquid-crystalline-based medium. *Angew. Chem., Int. Ed.* **2020**, *59*, 17097–17103.

(56) Qin, S. Y.; Ding, W. Q.; Jiang, Z. W.; Lei, X. X.; Zhang, A. Q. Directing an oligopeptide amphiphile into an aligned nanofiber matrix for elucidating molecular structures. *Chem. Commun. (Cambridge, U. K.)* **2019**, *55*, 1659–1662.

(57) Kobzar, K.; Luy, B. Analyses, extensions and comparison of three experimental schemes for measuring ((n)J(CH)+D-CH)-couplings at natural abundance. *J. Magn. Reson.* **2007**, *186*, 131–141.

(58) Trigo-Mouriño, P.; Navarro-Vázquez, A.; Ying, J.; Gil, R. R.; Bax, A. Structural discrimination in small molecules by accurate measurement of long-range proton-carbon NMR residual dipolar couplings. *Angew. Chem., Int. Ed.* **2011**, *50*, 7576–7580.

(59) Sauepe, A.; Englert, G. High-resolution nuclear magnetic resonance spectra of oriented molecules. *Phys. Rev. Lett.* **1963**, *11*, 462–464.

(60) Tycko, R.; Blanco, F. J.; Ishii, Y. Alignment of biopolymers in strained gels: A new way to create detectable dipole-dipole couplings in high-resolution biomolecular NMR. *J. Am. Chem. Soc.* **2000**, *122*, 9340–9341.

(61) Sass, H.-J.; Musco, G.; Stahl, S. J.; Wingfield, P. T.; Grzesiek, S. Solution NMR of proteins within polyacrylamide gels: Diffusional properties and residual alignment by mechanical stress or embedding of oriented purple membranes. *J. Biomol. NMR* **2000**, *18*, 303–309.

(62) Bothner-By, A. A.; Gayathri, C.; Vanzijl, P. C. M.; Maclean, C.; Lai, J. J.; Smith, K. M. High-field orientation effects in the high-resolution proton NMR spectra of diverse porphyrins. *Magn. Reson. Chem.* **1985**, *23*, 935–938.

(63) Tolman, J. R.; Flanagan, J. M.; Kennedy, M. A.; Prestegard, J. H. Nuclear magnetic dipole interactions in field-oriented proteins - Information for structure determination in solution. *Proc. Natl. Acad. Sci. U. S. A.* **1995**, *92*, 9279–9283.

(64) Tjandra, N.; Grzesiek, S.; Bax, A. Magnetic field dependence of nitrogen-proton J splittings in N-15-enriched human ubiquitin resulting from relaxation interference and residual dipolar coupling. *J. Am. Chem. Soc.* **1996**, *118*, 6264–6272.

(65) Vanzijl, P. C. M.; Ruessink, B. H.; Bulthuis, J.; Maclean, C. NMR of partially aligned liquids - Magnetic susceptibility anisotropies and dielectric properties. *Acc. Chem. Res.* **1984**, *17*, 172–180.

(66) Peshkovsky, A.; McDermott, A. E. NMR spectroscopy in the presence of strong ac electric fields: Degree of alignment of polar molecules. *J. Phys. Chem. A* **1999**, *103*, 8604–8611.

(67) Algeri, C.; Castiglione, F.; Celebre, G.; De Luca, G.; Longeri, M.; Emsley, J. W. The structure of ethylbenzene as a solute in liquid crystalline solvents via analysis of proton NMR spectra. *Phys. Chem. Chem. Phys.* **2000**, *2*, 3405–3413.

(68) Sinton, S.; Pines, A. Study of liquid crystal conformation by multiple quantum NMR - Normal-pentyl cyanobiphenyl. *Chem. Phys. Lett.* **1980**, *76*, 263–267.

(69) Gayathri, C.; Bothnerby, A. A.; Vanzijl, P. C. M.; Maclean, C. Dipolar magnetic-field effects in NMR spectra of liquids. *Chem. Phys. Lett.* **1982**, *87*, 192–196.

(70) Tjandra, N.; Omichinski, J. G.; Gronenborn, A. M.; Clore, G. M.; Bax, A. Use of dipolar 1H-15N and 1H-13C couplings in the structure determination of magnetically oriented macromolecules in solution. *Nat. Struct. Biol.* **1997**, *4*, 732–738.

(71) Ying, F.; Grishaev, A.; Latham, M. P.; Pardi, A.; Bax, A. Magnetic field induced residual dipolar couplings of imino groups in nucleic acids from measurements at a single magnetic field. *J. Biomol. NMR* **2007**, *39*, 91–96.

(72) Rodriguez-Castaneda, F.; Haberz, P.; Leonov, A.; Griesinger, C. Paramagnetic tagging of diamagnetic proteins for solution NMR. *Magn. Reson. Chem.* **2006**, *44*, S10–S16.

(73) Bax, A.; Tjandra, N. High-resolution heteronuclear NMR of human ubiquitin in an aqueous liquid crystalline medium. *J. Biomol. NMR* **1997**, *10*, 289–292.

(74) Losonczi, J. A.; Prestegard, J. H. Improved dilute bicelle solutions for high-resolution NMR of biological macromolecules. *J. Biomol. NMR* **1998**, *12*, 447–451.

(75) Ottiger, M.; Bax, A. Characterization of magnetically oriented phospholipid micelles for measurement of dipolar couplings in macromolecules. *J. Biomol. NMR* **1998**, *12*, 361–372.

(76) Wang, H.; Eberstadt, M.; Olejniczak, E. T.; Meadows, R. P.; Fesik, S. W. A liquid crystalline medium for measuring residual dipolar couplings over a wide range of temperatures. *J. Biomol. NMR* **1998**, *12*, 443–446.

(77) Ravula, T.; Ramamoorthy, A. Magnetic alignment of polymer macro-nanodiscs enables residual-dipolar-coupling-based high-resolution structural studies by NMR. *Angew. Chem., Int. Ed.* **2019**, *58*, 14925–14928.

(78) Ravula, T.; Ramamoorthy, A. Synthesis, characterization, and nanodisc formation of non-ionic polymers. *Angew. Chem., Int. Ed.* **2021**, *60*, 16885–16888.

(79) Park, S. H.; Berkamp, S.; Cook, G. A.; Chan, M. K.; Viadiu, H.; Opella, S. J. Nanodiscs versus macrodiscs for NMR of membrane proteins. *Biochemistry* **2011**, *50*, 8983–8985.

(80) Cavagnero, S.; Dyson, H. J.; Wright, P. E. Improved low pH bicelle system for orienting macromolecules over a wide temperature range. *J. Biomol. NMR* **1999**, *13*, 387–391.

(81) Ruckert, M.; Otting, G. Alignment of biological macromolecules in novel nonionic liquid crystalline media for NMR experiments. *J. Am. Chem. Soc.* **2000**, *122*, 7793–7797.

(82) Valafar, H.; Mayer, K. L.; Bougault, C. M.; LeBlond, P. D.; Jenney, F. E.; Brereton, P. S.; Adams, M. W. W.; Prestegard, J. H. Backbone solution structures of proteins using residual dipolar couplings: application to a novel structural genomics target. *J. Struct. Funct. Genomics* **2004**, *5*, 241–254.

(83) Barrientos, L. G.; Dolan, C.; Gronenborn, A. M. Characterization of surfactant liquid crystal phases suitable for molecular alignment and measurement of dipolar couplings. *J. Biomol. NMR* **2000**, *16*, 329–337.

(84) Prosser, R. S.; Losonczi, J. A.; Shiyonovskaya, I. V. Use of a novel aqueous liquid crystalline medium for high-resolution NMR of macromolecules in solution. *J. Am. Chem. Soc.* **1998**, *120*, 11010–11011.

(85) Thiagarajan-Rosenkranz, P.; Draney, A. W.; Smrt, S. T.; Lorieau, J. L. A Positively Charged Liquid Crystalline Medium for Measuring Residual Dipolar Couplings in Membrane Proteins by NMR. *J. Am. Chem. Soc.* **2015**, *137*, 11932–11934.

(86) Maltsev, A. S.; Grishaev, A.; Roche, J.; Zasloff, M.; Bax, A. Improved cross validation of a static ubiquitin structure derived from high precision residual dipolar couplings measured in a drug-based liquid crystalline phase. *J. Am. Chem. Soc.* **2014**, *136*, 3752–3755.

- (87) Hansen, M. R.; Mueller, L.; Pardi, A. Tunable alignment of macromolecules by filamentous phage yields dipolar coupling interactions. *Nat. Struct. Biol.* **1998**, *5*, 1065–1074.
- (88) Hansen, M. R.; Hanson, P.; Pardi, A. Filamentous bacteriophage for aligning RNA, DNA, and proteins for measurement of nuclear magnetic resonance dipolar coupling interactions. *Methods Enzymol.* **2000**, *317*, 220–240.
- (89) Clore, G. M.; Starich, M. R.; Gronenborn, A. M. Measurement of residual dipolar couplings of macromolecules aligned in the nematic phase of a colloidal suspension of rod-shaped viruses. *J. Am. Chem. Soc.* **1998**, *120*, 10571–10572.
- (90) Barrientos, L. G.; Louis, J. M.; Gronenborn, A. M. Characterization of the cholesteric phase of filamentous bacteriophage fd for molecular alignment. *J. Magn. Reson.* **2001**, *149*, 154–158.
- (91) Ma, J. H.; Goldberg, G. I.; Tjandra, N. Weak alignment of biomacromolecules in collagen gels: An alternative way to yield residual dipolar couplings for NMR measurements. *J. Am. Chem. Soc.* **2008**, *130*, 16148–16149.
- (92) Denisov, A. Y.; Kloser, E.; Gray, D. G.; Mittermaier, A. K. Protein alignment using cellulose nanocrystals: practical considerations and range of application. *J. Biomol. NMR* **2010**, *47*, 195–204.
- (93) Fleming, K.; Gray, D.; Prasanna, S.; Matthews, S. Cellulose crystallites: A new and robust liquid crystalline medium for the measurement of residual dipolar couplings. *J. Am. Chem. Soc.* **2000**, *122*, 5224–5225.
- (94) Douglas, S. M.; Chou, J. J.; Shih, W. M. DNA-nanotube-induced alignment of membrane proteins for NMR structure determination. *Proc. Natl. Acad. Sci. U. S. A.* **2007**, *104*, 6644–6648.
- (95) Lorieau, J.; Yao, L. S.; Bax, A. Liquid crystalline phase of G-tetrad DNA for NMR study of detergent-solubilized proteins. *J. Am. Chem. Soc.* **2008**, *130*, 7536–7537.
- (96) Singh, H.; Shukla, M.; Rao, B. J.; Chary, K. V. R. Flagella as a novel alignment medium for the measurement of residual dipolar couplings in proteins. *Chem. Commun. (Cambridge, U. K.)* **2013**, *49*, 11403–11405.
- (97) Sass, J.; Cordier, F.; Hoffmann, A.; Rogowski, M.; Cousin, A.; Omichinski, J. G.; Lowen, H.; Grzesiek, S. Purple membrane induced alignment of biological macromolecules in the magnetic field. *J. Am. Chem. Soc.* **1999**, *121*, 2047–2055.
- (98) Koenig, B. W.; Hu, J. S.; Ottiger, M.; Bose, S.; Hendler, R. W.; Bax, A. NMR measurement of dipolar couplings in proteins aligned by transient binding to purple membrane fragments. *J. Am. Chem. Soc.* **1999**, *121*, 1385–1386.
- (99) Bernadó, P.; Barbieri, R.; Padrós, E.; Luchinat, C.; Pons, M. Lanthanide modulation of the orientation of macromolecules induced by purple membrane. *J. Am. Chem. Soc.* **2002**, *124*, 374–375.
- (100) Feeney, J.; Birdsall, B.; Bradbury, A. F.; Biekofsky, R. R.; Bayley, P. M. Calmodulin tagging provides a general method of using lanthanide induced magnetic field orientation to observe residual dipolar couplings in proteins in solution. *J. Biomol. NMR* **2001**, *21*, 41–48.
- (101) Wohnert, J.; Franz, K. J.; Nitz, M.; Imperiali, B.; Schwalbe, H. Protein alignment by a coexpressed lanthanide-binding tag for the measurement of residual dipolar couplings. *J. Am. Chem. Soc.* **2003**, *125*, 13338–13339.
- (102) Ma, C.; Opella, S. J. Lanthanide ions bind specifically to an added “EF-hand” and orient a membrane protein in micelles for solution NMR spectroscopy. *J. Magn. Reson.* **2000**, *146*, 381–384.
- (103) Wang, Y.; An, L.; Yang, Y.; Yao, L. Generating five independent molecular alignments for simultaneous protein structure and dynamics determination using nuclear magnetic resonance spectroscopy. *Anal. Chem.* **2020**, *92*, 15263–15269.
- (104) Joss, D.; Haussinger, D. Design and applications of lanthanide chelating tags for pseudocontact shift NMR spectroscopy with biomacromolecules. *Prog. Nucl. Magn. Reson. Spectrosc.* **2019**, *114*, 284–312.
- (105) Haussinger, D.; Huang, J. R.; Grzesiek, S. DOTA-M8: an extremely rigid, high-affinity lanthanide chelating tag for PCS NMR spectroscopy. *J. Am. Chem. Soc.* **2009**, *131*, 14761–14767.
- (106) Meier, S.; Haussinger, D.; Grzesiek, S. Charged acrylamide copolymer gels as media for weak alignment. *J. Biomol. NMR* **2002**, *24*, 351–356.
- (107) Sanders, C. R.; Schwonek, J. P. Characterization of magnetically orientable bilayers in mixtures of dihexanoylphosphatidylcholine and dimyristoylphosphatidylcholine by solid-state NMR. *Biochemistry* **1992**, *31*, 8898–8905.
- (108) Tjandra, N.; Bax, A. Direct measurement of distances and angles in biomolecules by NMR in a dilute liquid crystalline medium. *Science* **1997**, *278*, 1111–4.
- (109) Zweckstetter, M.; Bax, A. Prediction of sterically induced alignment in a dilute liquid crystalline phase: Aid to protein structure determination by NMR. *J. Am. Chem. Soc.* **2000**, *122*, 3791–3792.
- (110) Zweckstetter, M. NMR: prediction of molecular alignment from structure using the PALES software. *Nat. Protoc.* **2008**, *3*, 679–690.
- (111) Fernandes, M. X.; Bernado, P.; Pons, M.; Garcia de la Torre, J. An analytical solution to the problem of the orientation of rigid particles by planar obstacles. Application to membrane systems and to the calculation of dipolar couplings in protein NMR spectroscopy. *J. Am. Chem. Soc.* **2001**, *123*, 12037–12047.
- (112) Berlin, K.; O’Leary, D. P.; Fushman, D. Structural assembly of molecular complexes based on residual dipolar couplings. *J. Am. Chem. Soc.* **2010**, *132*, 8961–8972.
- (113) Ramirez, B. E.; Bax, A. Modulation of the alignment tensor of macromolecules dissolved in a dilute liquid crystalline medium. *J. Am. Chem. Soc.* **1998**, *120*, 9106–9107.
- (114) Zweckstetter, M.; Hummer, G.; Bax, A. Prediction of charge-induced molecular alignment of biomolecules dissolved in dilute liquid-crystalline phases. *Biophys. J.* **2004**, *86*, 3444–3460.
- (115) Seelig, J.; Borle, F.; Cross, T. A. Magnetic ordering of phospholipid membranes. *Biochim. Biophys. Acta, Biomembr.* **1985**, *814*, 195–198.
- (116) Speyer, J. B.; Sripada, P. K.; Dasgupta, S. K.; Shipley, G. G.; Griffin, R. G. Magnetic orientation of sphingomyelin lecithin bilayers. *Biophys. J.* **1987**, *51*, 687–691.
- (117) Ram, P.; Prestegard, J. H. Magnetic field induced ordering of bile salt/phospholipid micelles: new media for NMR structural investigations. *Biochim. Biophys. Acta, Biomembr.* **1988**, *940*, 289–294.
- (118) Sanders, C. R.; Hare, B. J.; Howard, K. P.; Prestegard, J. H. Magnetically-Oriented Phospholipid Micelles As a Tool For the Study of Membrane-Associated Molecules. *Prog. Nucl. Magn. Reson. Spectrosc.* **1994**, *26*, 421–444.
- (119) Struppe, J.; Vold, R. R. Dilute bicellar solutions for structural NMR work. *J. Magn. Reson.* **1998**, *135*, 541–546.
- (120) Chou, J. J.; Baber, J. L.; Bax, A. Characterization of phospholipid mixed micelles by translational diffusion. *J. Biomol. NMR* **2004**, *29*, 299–308.
- (121) Ramirez, B. E.; Voloshin, O. N.; Camerini-Otero, R. D.; Bax, A. Solution structure of DinI provides insight into its mode of RecA inactivation. *Protein Sci.* **2000**, *9*, 2161–2169.
- (122) Williams, D. E.; Grant, K. B. Metal-assisted hydrolysis reactions involving lipids: a review. *Front. Chem.* **2019**, *7*, 00014.
- (123) Deatherage, C. L.; Lu, Z.; Kroncke, B. M.; Ma, S.; Smith, J. A.; Voehler, M. W.; McFeeters, R. L.; Sanders, C. R. Structural and biochemical differences between the Notch and the amyloid precursor protein transmembrane domains. *Science advances* **2017**, *3*, No. e1602794.
- (124) Otting, G.; Widmer, H.; Wagner, G.; Wüthrich, K. Origin of  $t_1$  and  $t_2$  ridges in 2D NMR spectra and procedures for suppression. *J. Magn. Reson.* **1986**, *66*, 187–193.
- (125) Jonstromer, M.; Strey, R. Nonionic bilayers in dilute solutions - Effect of additives. *J. Phys. Chem.* **1992**, *96*, 5993–6000.
- (126) Liu, D. J.; Day, L. A. Pfl virus structure - helical coat protein and DNA with paraxial phosphates. *Science* **1994**, *265*, 671–674.
- (127) Zimmermann, K.; Hagedorn, H.; Heuck, C. C.; Hinrichsen, M.; Ludwig, H. The ionic properties of the filamentous bacteriophages Pfl and fd. *J. Biol. Chem.* **1986**, *261*, 1653–1655.

- (128) Zweckstetter, M.; Bax, A. Characterization of molecular alignment in aqueous suspensions of Pfl bacteriophage. *J. Biomol. NMR* **2001**, *20*, 365–377.
- (129) Chou, J. J.; Gaemers, S.; Howder, B.; Louis, J. M.; Bax, A. A simple apparatus for generating stretched polyacrylamide gels, yielding uniform alignment of proteins and detergent micelles. *J. Biomol. NMR* **2001**, *21*, 377–382.
- (130) Cierpicki, T.; Bushweller, J. H. Charged gels as orienting media for measurement of residual dipolar couplings in soluble and integral membrane proteins. *J. Am. Chem. Soc.* **2004**, *126*, 16259–16266.
- (131) Ulmer, T. S.; Ramirez, B. E.; Delaglio, F.; Bax, A. Evaluation of backbone proton positions and dynamics in a small protein by liquid crystal NMR spectroscopy. *J. Am. Chem. Soc.* **2003**, *125*, 9179–9191.
- (132) Mehlkopf, A. F.; Korbee, D.; Tiggelman, T. A.; Freeman, R. Sources of t1 noise in two-dimensional NMR. *J. Magn. Reson.* **1984**, *58*, 315–323.
- (133) Kay, L. E.; Keifer, P.; Saarinen, T. Pure absorption gradient-enhanced heteronuclear single quantum correlation spectroscopy with improved sensitivity. *J. Am. Chem. Soc.* **1992**, *114*, 10663–10665.
- (134) Bertini, I.; Janik, M. B. L.; Lee, Y.-M.; Luchinat, C.; Rosato, A. Magnetic susceptibility tensor anisotropies for a lanthanide ion series in a fixed protein matrix. *J. Am. Chem. Soc.* **2001**, *123*, 4181–4188.
- (135) Su, X. C.; Otting, G. Paramagnetic labelling of proteins and oligonucleotides for NMR. *J. Biomol. NMR* **2010**, *46*, 101–112.
- (136) Su, X.-C.; McAndrew, K.; Huber, T.; Otting, G. Lanthanide-binding peptides for NMR measurements of residual dipolar couplings and paramagnetic effects from multiple angles. *J. Am. Chem. Soc.* **2008**, *130*, 1681–1687.
- (137) Kamen, D. E.; Cahill, S. M.; Girvin, M. E. Multiple alignment of membrane proteins for measuring residual dipolar couplings using lanthanide ions bound to a small metal chelator. *J. Am. Chem. Soc.* **2007**, *129*, 1846–1847.
- (138) Opina, A. C. L.; Strickland, M.; Lee, Y. S.; Tjandra, N.; Byrd, R. A.; Swenson, R. E.; Vasalatiy, O. Analysis of the isomer ratios of polymethylated-DOTA complexes and the implications on protein structural studies. *Dalton Trans.* **2016**, *45*, 4673–4687.
- (139) Müntener, T.; Kottelat, J.; Huber, A.; Häussinger, D. New lanthanide chelating tags for PCS NMR spectroscopy with reduction stable, rigid linkers for fast and irreversible conjugation to proteins. *Bioconjugate Chem.* **2018**, *29*, 3344–3351.
- (140) Schmitz, C.; Stanton-Cook, M. J.; Su, X.-C.; Otting, G.; Huber, T. Nubat: an interactive software tool for fitting  $\Delta\gamma$ -tensors to molecular coordinates using pseudocontact shifts. *J. Biomol. NMR* **2008**, *41*, 179.
- (141) Pintacuda, G.; Keniry, M. A.; Huber, T.; Park, A. Y.; Dixon, N. E.; Otting, G. Fast structure-based assignment of 15N HSQC spectra of selectively 15N-labeled paramagnetic proteins. *J. Am. Chem. Soc.* **2004**, *126*, 2963–2970.
- (142) Otting, G. Protein NMR using paramagnetic ions. *Annu. Rev. Biophys.* **2010**, *39*, 387–405.
- (143) Banci, L.; Bertini, I.; Savellini, G. G.; Romagnoli, A.; Turano, P.; Cremonini, M. A.; Luchinat, C.; Gray, H. B. Pseudocontact shifts as constraints for energy minimization and molecular dynamics calculations on solution structures of paramagnetic metalloproteins. *Proteins: Struct., Funct., Genet.* **1997**, *29*, 68–76.
- (144) Gochin, M.; Roder, H. Protein structure refinement based on paramagnetic NMR shifts - Applications to wild-type and mutant forms of cytochrome C. *Protein Sci.* **1995**, *4*, 296–305.
- (145) Allen, K. N.; Imperiali, B. Lanthanide-tagged proteins - an illuminating partnership. *Curr. Opin. Chem. Biol.* **2010**, *14*, 247–254.
- (146) Iwahara, J.; Anderson, D. E.; Murphy, E. C.; Clore, G. M. EDTA-derivatized deoxythymidine as a tool for rapid determination of protein binding polarity to DNA by intermolecular paramagnetic relaxation enhancement. *J. Am. Chem. Soc.* **2003**, *125*, 6634–6635.
- (147) Cheng, Y.; Patel, D. J. An efficient system for small protein expression and refolding. *Biochem. Biophys. Res. Commun.* **2004**, *317*, 401–405.
- (148) Zhou, P.; Wagner, G. Overcoming the solubility limit with solubility-enhancement tags: successful applications in biomolecular NMR studies. *J. Biomol. NMR* **2010**, *46*, 23–31.
- (149) Moltke, S.; Grzesiek, S. Structural constraints from residual tensorial couplings in high resolution NMR without an explicit term for the alignment tensor. *J. Biomol. NMR* **1999**, *15*, 77–82.
- (150) Carlon, A.; Ravera, E.; Hennig, J.; Parigi, G.; Sattler, M.; Luchinat, C. Improved accuracy from joint X-ray and NMR refinement of a protein-RNA complex structure. *J. Am. Chem. Soc.* **2016**, *138*, 1601–1610.
- (151) Delaglio, F.; Kontaxis, G.; Bax, A. Protein structure determination using Molecular Fragment Replacement and NMR dipolar couplings. *J. Am. Chem. Soc.* **2000**, *122*, 2142–2143.
- (152) Simon, B.; Sattler, M. De novo structure determination from residual dipolar couplings by NMR spectroscopy. *Angew. Chem., Int. Ed.* **2002**, *41*, 437–440.
- (153) Senior, A. W.; Evans, R.; Jumper, J.; Kirkpatrick, J.; Sifre, L.; Green, T.; Qin, C.; Židek, A.; Nelson, A. W. R.; Bridgland, A.; Penedones, H.; Petersen, S.; Simonyan, K.; Crossan, S.; Kohli, P.; Jones, D. T.; Silver, D.; Kavukcuoglu, K.; Hassabis, D. Improved protein structure prediction using potentials from deep learning. *Nature* **2020**, *577*, 706–710.
- (154) Baek, M.; DiMaio, F.; Anishchenko, I.; Dauparas, J.; Ovchinnikov, S.; Lee, G. R.; Wang, J.; Cong, Q.; Kinch, L. N.; Schaeffer, R. D.; et al. Accurate prediction of protein structures and interactions using a three-track neural network. *Science* **2021**, *373*, 871–876.
- (155) Jumper, J.; Evans, R.; Pritzel, A.; Green, T.; Figurnov, M.; Ronneberger, O.; Tunyasuvunakool, K.; Bates, R.; Židek, A.; Potapenko, A.; et al. Highly accurate protein structure prediction with AlphaFold. *Nature* **2021**, *596*, 583–589.
- (156) Miclet, E.; O'Neil-Cabello, E.; Nikonowicz, E. P.; Live, D.; Bax, A. H-1-H-1 dipolar couplings provide a unique probe of RNA backbone structure. *J. Am. Chem. Soc.* **2003**, *125*, 15740–15741.
- (157) Miclet, E.; Boisbouvier, J.; Bax, A. Measurement of eight scalar and dipolar couplings for methine-methylene pairs in proteins and nucleic acids. *J. Biomol. NMR* **2005**, *31*, 201–216.
- (158) Bax, A.; Vuister, G. W.; Grzesiek, S.; Delaglio, F.; Wang, A. C.; Tschudin, R.; Zhu, G. Measurement of homonuclear and heteronuclear J-couplings from quantitative J-correlation. *Methods Enzymol.* **1994**, *239*, 79–105.
- (159) Ottiger, M.; Delaglio, F.; Bax, A. Measurement of J and dipolar couplings from simplified two-dimensional NMR spectra. *J. Magn. Reson.* **1998**, *131*, 373–8.
- (160) Yao, L. S.; Ying, J. F.; Bax, A. Improved accuracy of N-15-H-1 scalar and residual dipolar couplings from gradient-enhanced IPAP-HSQC experiments on protonated proteins. *J. Biomol. NMR* **2009**, *43*, 161–170.
- (161) Kontaxis, G.; Clore, G. M.; Bax, A. Evaluation of cross-correlation effects and measurement of one-bond couplings in proteins with short transverse relaxation times. *J. Magn. Reson.* **2000**, *143*, 184–196.
- (162) Tolman, J. R.; Prestegard, J. H. A quantitative J-correlation experiment for the accurate measurement of one-bond amide N-15-H-1 couplings in proteins. *J. Magn. Reson., Ser. B* **1996**, *112*, 245–252.
- (163) Tjandra, N.; Bax, A. Measurement of dipolar contributions to 1JCH splittings from magnetic-field dependence of J modulation in two-dimensional NMR spectra. *J. Magn. Reson.* **1997**, *124*, 512–5.
- (164) Pervushin, K.; Riek, R.; Wider, G.; Wuthrich, K. Attenuated T2 relaxation by mutual cancellation of dipole-dipole coupling and chemical shift anisotropy indicates an avenue to NMR structures of very large biological macromolecules in solution. *Proc. Natl. Acad. Sci. U. S. A.* **1997**, *94*, 12366–12371.
- (165) Salzman, M.; Wider, G.; Pervushin, K.; Senn, H.; Wuthrich, K. TROSY-type triple-resonance experiments for sequential NMR assignments of large proteins. *J. Am. Chem. Soc.* **1999**, *121*, 844–848.
- (166) Eletsky, A.; Pulavarti, S. V. S. R. K.; Beaumont, V.; Gollnick, P.; Szyperski, T. Solution NMR experiment for measurement of 15N-

- <sup>1</sup>H residual dipolar couplings in large proteins and supramolecular complexes. *J. Am. Chem. Soc.* **2015**, *137*, 11242–11245.
- (167) Wang, Y. X.; Marquardt, J. L.; Wingfield, P.; Stahl, S. J.; Lee-Huang, S.; Torchia, D.; Bax, A. Simultaneous measurement of H-1-N-15, H-1-C-13', and N-15-C-13' dipolar couplings in a perdeuterated 30 kDa protein dissolved in a dilute liquid crystalline phase. *J. Am. Chem. Soc.* **1998**, *120*, 7385–7386.
- (168) Ottiger, M.; Bax, A. Determination of relative N-H-N N-C', C-alpha-C' and C(alpha)-H-alpha effective bond lengths in a protein by NMR in a dilute liquid crystalline phase. *J. Am. Chem. Soc.* **1998**, *120*, 12334–12341.
- (169) Ying, J.; Delaglio, F.; Torchia, D. A.; Bax, A. Sparse multidimensional iterative lineshape-enhanced (SMILE) reconstruction of both non-uniformly sampled and conventional NMR data. *J. Biomol. NMR* **2017**, *68*, 101–118.
- (170) Jaroniec, C. P.; Ulmer, T. S.; Bax, A. Quantitative J correlation methods for the accurate measurement of <sup>13</sup>C'-<sup>13</sup>C $\alpha$ dipolar couplings in proteins. *J. Biomol. NMR* **2004**, *30*, 181–194.
- (171) Yamazaki, T.; Tochio, H.; Furui, J.; Aimoto, S.; Kyogoku, Y. Assignment of Backbone Resonances for Larger Proteins Using the <sup>13</sup>C-1H Coherence of a 1H $\alpha$ -, 2H-, <sup>13</sup>C-, and <sup>15</sup>N-Labeled Sample. *J. Am. Chem. Soc.* **1997**, *119*, 872–880.
- (172) Movellan, K. T.; Najbauer, E. E.; Pratihari, S.; Salvi, M.; Giller, K.; Becker, S.; Andreas, L. B. Alpha protons as NMR probes in deuterated proteins. *J. Biomol. NMR* **2019**, *73*, 81–91.
- (173) Grzesiek, S.; Bax, A. Correlating backbone amide and side chain resonances in larger proteins by multiple relayed triple resonance NMR. *J. Am. Chem. Soc.* **1992**, *114*, 6291–6293.
- (174) Chou, J. J.; Bax, A. Protein side-chain rotamers from dipolar couplings in a liquid crystalline phase. *J. Am. Chem. Soc.* **2001**, *123*, 3844–3845.
- (175) Doddrell, D. M.; Pegg, D. T.; Bendall, M. R. Distortionless Enhancement of NMR Signals by Polarization Transfer. *J. Magn. Reson.* **1982**, *48*, 323–327.
- (176) Mittermaier, A.; Kay, L. E.  $\chi(1)$  torsion angle dynamics in proteins from dipolar couplings. *J. Am. Chem. Soc.* **2001**, *123*, 6892–6903.
- (177) Li, F.; Grishaev, A.; Ying, J.; Bax, A. Side-chain conformational distributions of a small protein derived from model-free analysis of a large set of residual dipolar couplings. *J. Am. Chem. Soc.* **2015**, *137*, 14798–14811.
- (178) Ramanujam, V.; Shen, Y.; Ying, J. F.; Mobli, M. Residual dipolar couplings for resolving cysteine bridges in disulfide-rich peptides. *Front. Chem.* **2020**, *7*, 13.
- (179) Dzakula, Z.; Edison, A. S.; Westler, W. M.; Markley, J. L. Analysis of  $\chi(1)$  rotamer populations from NMR data by the CUPID method. *J. Am. Chem. Soc.* **1992**, *114*, 6200–6207.
- (180) Perez, C.; Lohr, F.; Ruterjans, H.; Schmidt, J. M. Self-consistent Karplus parametrization of (<sup>3</sup>J) couplings depending on the polypeptide side-chain torsion  $\chi(1)$ . *J. Am. Chem. Soc.* **2001**, *123*, 7081–7093.
- (181) Rosen, M. K.; Gardner, K. H.; Willis, R. C.; Parris, W. E.; Pawson, T.; Kay, L. E. Selective methyl group protonation of perdeuterated proteins. *J. Mol. Biol.* **1996**, *263*, 627–636.
- (182) Toyama, Y.; Harkness, R. W.; Lee, T. Y. T.; Maynes, J. T.; Kay, L. E. Oligomeric assembly regulating mitochondrial HtrA2 function as examined by methyl-TROSY NMR. *Proc. Natl. Acad. Sci. U. S. A.* **2021**, *118*, e2025022118.
- (183) Macek, P.; Kerfah, R.; Erba, E. B.; Crublet, E.; Moriscot, C.; Schoehn, G.; Amero, C.; Boisbouvier, J. Unraveling self-assembly pathways of the 468-kDa proteolytic machine TET2. *Sci. Adv.* **2017**, *3*, e1601601.
- (184) Behera, S. P.; Dubey, A.; Chen, W. N.; De Paula, V. S.; Zhang, M.; Sgourakis, N. G.; Bermel, W.; Wagner, G.; Coote, P. W.; Arthanari, H. Nearest-neighbor NMR spectroscopy: categorizing spectral peaks by their adjacent nuclei. *Nat. Commun.* **2020**, *11*, 5547.
- (185) Pederson, K.; Chalmers, G. R.; Gao, Q.; Elnatan, D.; Ramelot, T. A.; Ma, L.-C.; Montelione, G. T.; Kennedy, M. A.; Agard, D. A.; Prestegard, J. H. NMR characterization of HtpG, the E. coli Hsp90, using sparse labeling with <sup>13</sup>C-methyl alanine. *J. Biomol. NMR* **2017**, *68*, 225–236.
- (186) Ottiger, M.; Bax, A. How tetrahedral are methyl groups in proteins? A liquid crystal NMR study. *J. Am. Chem. Soc.* **1999**, *121*, 4690–4695.
- (187) Kontaxis, G.; Bax, A. Multiplet component separation for measurement of methyl C-13- H-1 dipolar couplings in weakly aligned proteins. *J. Biomol. NMR* **2001**, *20*, 77–82.
- (188) Salmon, L.; Yang, S.; Al-Hashimi, H. M. Advances in the determination of nucleic acid conformational ensembles. *Annu. Rev. Phys. Chem.* **2014**, *65*, 293–316.
- (189) Sibille, N.; Pardi, A.; Simorre, J. P.; Blackledge, M. Refinement of local and long-range structural order in theophylline-binding RNA using C-13-H-1 residual dipolar couplings and restrained molecular dynamics. *J. Am. Chem. Soc.* **2001**, *123*, 12135–12146.
- (190) Getz, M.; Sun, X. Y.; Casiano-Negroni, A.; Zhang, Q.; Al-Hashimi, H. M. NMR studies of RNA dynamics and structural plasticity using NMR residual dipolar couplings. *Biopolymers* **2007**, *86*, 384–402.
- (191) Ying, J.; Wang, J.; Grishaev, A.; Yu, P.; Wang, Y.-X.; Bax, A. Measurement of (<sup>1</sup>H)-(<sup>15</sup>N) and (<sup>1</sup>H)-(<sup>13</sup>C) residual dipolar couplings in nucleic acids from TROSY intensities. *J. Biomol. NMR* **2011**, *51*, 89–103.
- (192) Sanders, C. R.; Prestegard, J. H. Orientation and dynamics of beta-dodecyl glucopyranoside in phospholipid-bilayers by oriented sample NMR and order matrix analysis. *J. Am. Chem. Soc.* **1991**, *113*, 1987–1996.
- (193) Losonczi, J. A.; Andrec, M.; Fischer, M. W. F.; Prestegard, J. H. Order matrix analysis of residual dipolar couplings using singular value decomposition. *J. Magn. Reson.* **1999**, *138*, 334–342.
- (194) Bax, A.; Kontaxis, G.; Tjandra, N. Dipolar couplings in macromolecular structure determination. *Methods Enzymol.* **2001**, *339*, 127–174.
- (195) Clore, G. M.; Gronenborn, A. M.; Bax, A. A robust method for determining the magnitude of the fully asymmetric alignment tensor of oriented macromolecules in the absence of structural information. *J. Magn. Reson.* **1998**, *133*, 216–21.
- (196) Zweckstetter, M.; Bax, A. Evaluation of uncertainty in alignment tensors obtained from dipolar couplings. *J. Biomol. NMR* **2002**, *23*, 127–137.
- (197) Fushman, D.; Ghose, R.; Cowburn, D. The effect of finite sampling on the determination of orientational properties: A theoretical treatment with application to interatomic vectors in proteins. *J. Am. Chem. Soc.* **2000**, *122*, 10640–10649.
- (198) Brunger, A. T. Free R-value - a novel statistical quantity for assessing the accuracy of crystal-structures. *Nature* **1992**, *355*, 472–475.
- (199) Lorieau, J. L.; Maltsev, A. S.; Louis, J. M.; Bax, A. Modulating alignment of membrane proteins in liquid-crystalline and oriented gel media by changing the size and charge of phospholipid bicelles. *J. Biomol. NMR* **2013**, *55*, 369–377.
- (200) Koradi, R.; Billeter, M.; Wuthrich, K. MOLMOL: a program for display and analysis of macromolecular structures. *J. Mol. Graphics* **1996**, *14*, 51–55.
- (201) Delaglio, F.; Grzesiek, S.; Vuister, G. W.; Zhu, G.; Pfeifer, J.; Bax, A. NMRpipe - a multidimensional spectral processing system based on Unix pipes. *J. Biomol. NMR* **1995**, *6*, 277–293.
- (202) Schwieters, C. D.; Kuszewski, J. J.; Clore, G. M. Using Xplor-NIH for NMR molecular structure determination. *Prog. Nucl. Magn. Reson. Spectrosc.* **2006**, *48*, 47–62.
- (203) Chen, V. B.; Arendall, W. B., III; Headd, J. J.; Keedy, D. A.; Immormino, R. M.; Kapral, G. J.; Murray, L. W.; Richardson, J. S.; Richardson, D. C. MolProbity: all-atom structure validation for macromolecular crystallography. *Acta Crystallogr., Sect. D: Biol. Crystallogr.* **2010**, *66*, 12–21.
- (204) Lipari, G.; Szabo, A. Model-free approach to the interpretation of nuclear magnetic resonance relaxation in macromolecules. 1. Theory and range of validity. *J. Am. Chem. Soc.* **1982**, *104*, 4546–4559.

- (205) Torchia, D. A. NMR studies of dynamic biomolecular conformational ensembles. *Prog. Nucl. Magn. Reson. Spectrosc.* **2015**, *84*, 14–32.
- (206) Palmer, A. G. NMR characterization of the dynamics of biomacromolecules. *Chem. Rev.* **2004**, *104*, 3623–3640.
- (207) Mittermaier, A.; Kay, L. E. Review - New tools provide new insights in NMR studies of protein dynamics. *Science* **2006**, *312*, 224–228.
- (208) Palmer, A. G.; Koss, H. Chemical exchange. *Methods Enzymol.* **2019**, *615*, 177–236.
- (209) Li, T.; Jing, Q.; Yao, L. Dynamics of the GB3 loop regions from MD simulation: How much of it is real? *J. Phys. Chem. B* **2011**, *115*, 3488–3495.
- (210) Baldwin, A. J.; Hansen, D. F.; Vallurupalli, P.; Kay, L. E. Measurement of methyl axis orientations in invisible, excited states of proteins by relaxation dispersion NMR spectroscopy. *J. Am. Chem. Soc.* **2009**, *131*, 11939–11948.
- (211) Hus, J. C.; Bruschweiler, R. Principal component method for assessing structural heterogeneity across multiple alignment media. *J. Biomol. NMR* **2002**, *24*, 123–132.
- (212) Yao, L.; Vogeli, B.; Torchia, D. A.; Bax, A. Simultaneous NMR study of protein structure and dynamics using conservative mutagenesis. *J. Phys. Chem. B* **2008**, *112*, 6045–6056.
- (213) Lorieau, J. L.; Louis, J. M.; Bax, A. The complete influenza hemagglutinin fusion domain adopts a tight helical hairpin arrangement at the lipid:water interface. *Proc. Natl. Acad. Sci. U. S. A.* **2010**, *107*, 11341–11346.
- (214) Zhang, Q.; Stelzer, A. C.; Fisher, C. K.; Al-Hashimi, H. M. Visualizing spatially correlated dynamics that directs RNA conformational transitions. *Nature* **2007**, *450*, 1263–1267.
- (215) Bernado, P.; Bertocini, C. W.; Griesinger, C.; Zweckstetter, M.; Blackledge, M. Defining long-range order and local disorder in native alpha-synuclein using residual dipolar couplings. *J. Am. Chem. Soc.* **2005**, *127*, 17968–17969.
- (216) Bernado, P.; Blanchard, L.; Timmins, P.; Marion, D.; Ruigrok, R. W. H.; Blackledge, M. A structural model for unfolded proteins from residual dipolar couplings and small-angle x-ray scattering. *Proc. Natl. Acad. Sci. U. S. A.* **2005**, *102*, 17002–17007.
- (217) Huang, J. R.; Grzesiek, S. Ensemble calculations of unstructured proteins constrained by RDC and PRE data: A case study of urea-denatured ubiquitin. *J. Am. Chem. Soc.* **2010**, *132*, 694–705.
- (218) Jensen, M. R.; Communie, G.; Ribeiro, E. A.; Martinez, N.; Desfosses, A.; Salmon, L.; Mollica, L.; Gabel, F.; Jamin, M.; Longhi, S.; et al. Intrinsic disorder in measles virus nucleocapsids. *Proc. Natl. Acad. Sci. U. S. A.* **2011**, *108*, 9839.
- (219) Chou, J. J.; Li, S.; Klee, C. B.; Bax, A. Solution structure of Ca<sup>2+</sup>-calmodulin reveals flexible hand-like properties of its domains. *Nat. Struct. Biol.* **2001**, *8*, 990–997.
- (220) Sun, Y. J.; Goldman, Y. E. Lever-Arm Mechanics of Processive Myosins. *Biophys. J.* **2011**, *101*, 1–11.
- (221) Batchelor, M.; Wolny, M.; Baker, E. G.; Paci, E.; Kalverda, A. P.; Peckham, M. Dynamic ion pair behavior stabilizes single alpha helices in proteins. *J. Biol. Chem.* **2019**, *294*, 3219–3234.
- (222) Huang, S. K.; Pandey, A.; Tran, D. P.; Villanueva, N. L.; Kitao, A.; Sunahara, R. K.; Sljoka, A.; Prosser, R. S. Delineating the conformational landscape of the adenosine A(2A) receptor during G protein coupling. *Cell* **2021**, *184*, 1884–1894.
- (223) Isogai, S.; Deupi, X.; Opitz, C.; Heydenreich, F. M.; Tsai, C.-J.; Brueckner, F. B.; Schertler, G. F. X.; Vepintsev, D. B.; Grzesiek, S. Backbone NMR reveals allosteric signal transduction networks in the beta(1)-adrenergic receptor. *Nature* **2016**, *530*, 237–241.
- (224) Clore, G. M.; Iwahara, J. Theory, practice, and applications of paramagnetic relaxation enhancement for the characterization of transient low-population states of biological macromolecules and their complexes. *Chem. Rev.* **2009**, *109*, 4108–4139.
- (225) Bertini, I.; Kursula, P.; Luchinat, C.; Parigi, G.; Vahokoski, J.; Wilmanns, M.; Yuan, J. Accurate solution structures of proteins from X-ray data and a minimal set of NMR data: calmodulin-peptide complexes as examples. *J. Am. Chem. Soc.* **2009**, *131*, 5134–5144.
- (226) Koehler, J.; Meiler, J. Expanding the utility of NMR restraints with paramagnetic compounds: Background and practical aspects. *Prog. Nucl. Magn. Reson. Spectrosc.* **2011**, *59*, 360–389.
- (227) Gaalswyk, K.; Liu, Z.; Vogel, H. J.; MacCallum, J. L. An integrative approach to determine 3D protein structures using sparse paramagnetic NMR data and physical modeling. *Front. Mol. Biosci.* **2021**, *8*, 676268.